the cells were inoculated with the HIV-1 (60 MAGI U/well, giving 60 blue cells after 48 h of incubation) and cultured in the presence of various concentrations of the drugs in fresh medium. Forty-eight hours after viral exposure, all the blue cells stained with X-Gal (5-bromo-4-chloro-3-indolyl-β-D-galactopyranoside) were counted in each well. The activity of test compounds was determined as the concentration that blocked HIV-1 replication by 50% (50% effective concentration [EC_{50}]).

Acknowledgements

This work was supported by Grants-in-Aid for Scientific Research from MEXT, Japan, and Health and Labour Science Research Grants (Research on HIV/AIDS). T.N. and K.T. are grateful for the JSPS Research Fellowships for Young Scientists. We are grateful to Prof. Hirokazu Tamamura and Mr. Tomohiro Tanaka for helpful discussions.

References

1 (*a*) M. Loetscher, T. Geiser, T. O'Reilly, R. Zwahlen, M. Baggiolini and B. Moser, *J. Biol. Chem*, 1994, **269**, 232–237; (*b*) B. J. Rollins, *Blood*, 1997, **90**, 909–928.

2 (*a*) T. Nagasawa, S. Hirota, K. Tachibana, N. Takakura, S. Nishikawa, Y. Kitamura, N. Yoshida, H. Kikutani and T. Kishimoto, *Nature*, 1996, **382**, 635–638; (*b*) K. Tachibana, S. Hirota, H. Iizasa, H. Yoshida, K. Kawabata, Y. Kataoka, Y. Kitamura, K. Matsushima, N. Yoshida, S. Nishikawa, T. Kishimoto and T. Nagasawa, *Nature*, 1998, **393**, 591–594.

3 C. C. Bleul, R. C. Fuhlbrigge, J. M. Casanovas, A. Aiuti and T. A. Springer, *J. Exp. Med.*, 1996, **184**, 1101–1109.

4 (*a*) Y. Zhu, Y. Yu, X. C. Zhang, T. Nagasawa, J. Y. Wu and Y. Rao, *Nat. Neurosci.*, 2002, **5**, 513–720; (*b*) R. K. Stumm, C. Zhou, T. Ara, F. Lazarini, M. Dubois-Dalcq, T. Nagasawa, V. Hollt and S. Schulz, *J. Neurosci.*, 2003, **23**, 5123–5130.

5 (*a*) A. Müller, B. Homey, H. Soto, N. Ge, D. Catron, M. E. Buchanan, T. Mcclanahan, E. Murphy, W. Yuan, S. M. Wagner, J. L. Barrera, A. Mohar, E. Verástegui and A. Zlotnik, *Nature*, 2001, **410**, 50–56; (*b*) J. A. Burger, M. Burger and T. J. Kipps, *Blood*, 1999, **94**, 3658–3667.

6 Y. Feng, C. C. Broder, P. E. Kennedy and E. A. Berger, *Science*, 1996, **272**, 872–877.

7 T. Nanki, K. Hayashida, H. S. EI-Gabalawy, S. Suson, K. Shi, H. J. Girschick, S. Yavuz and P. E. Lipsky, *J. Immunol.*, 2000, **165**, 6590–6598.

8 (*a*) T. Murakami, T. Nakajima, Y. Koyanagi, K. Tachibana, N. Fujii, H. Tamamura, N. Yoshida, M. Waki, A. Matsumoto, O. Yoshie, T. Kishimoto, N. Yamamoto and T. Nagasawa, *J. Exp. Med.*, 1997, **186**, 1389–1393; (*b*) D. Schols, S. Struyf, J. Van Damme, J. A. Este, G. Henson and E. De Clercq, *J. Exp. Med.*, 1997, **186**, 1383–1388; (*c*) G. A. Donzella, D. Schols, S. W. Lin, J. A. Este, K. A. Nagashima, P. J. Maddon, G. P. Allaway, T. P. Sakmar, G. Henson, E. De Clercq and J. P. Moore, *Nat. Med.*, 1998, **4**, 72–77; (*d*) B. J. Doranz, K. Grovit-Ferbas, M. P. Sharron, S.-H. Mao, M. Bidwell Goetz, E. S. Daar, R. W. Doms and W. A. O'Brien, *J. Exp. Med.*, 1997, **186**, 1395–1400; (*e*) O. M. Z. Howard, J. J. Oppenheim, M. G. Hollingshead, J. M. Covey, J. Bigelow, J. J. McCormack, R. W. Buckheit Jr., D. J. Clanton, J. A. Turpin and W. G. Rice, *J. Med. Chem.*, 1998, **41**, 2184–2193.

9 For recent reviews, see:(*a*) H. Shim, S. Oishi and N. Fujii, *Semin. Cancer Biol.*, 2009, **19**, 123–134; (*b*) E. De Clercq, *Biochem. Pharmacol.*, 2009, **77**, 1655–1664.

10 (*a*) H. Tamamura, A. Omagari, S. Oishi, T. Kanamoto, N. Yamamoto, S. C. Peiper, H. Nakashima, A. Otaka and N. Fujii, *Bioorg. Med. Chem. Lett.*, 2000, **10**, 2633–2637; (*b*) H. Tamamura, Y. Sugioka, A. Odagaki, A. Omagari, Y. Kan, S. Oishi, H. Nakashima, N. Yamamoto, S. C. Peiper, A. Hamanaka, A. Otaka and N. Fujii, *Bioorg. Med. Chem. Lett.*, 2001, **11**, 359–362.

11 N. Fujii, S. Oishi, K. Hiramatsu, T. Araki, S. Ueda, H. Tamamura, A. Otaka, S. Kusano, S. Terakubo, H. Nakashima, J. A. Broach, J. O. Trent, Z. Wang and S. C. Peiper, *Angew. Chem., Int. Ed.*, 2003, **42**, 3251–3253.

12 (*a*) H. Tamamura, A. Esaka, T. Ogawa, T. Araki, S. Ueda, Z. Wang, J. O. Trent, H. Tsutsumi, H. Masuno, H. Nakashima, N. Yamamoto, S. C. Peiper, A. Otaka and N. Fujii, *Org. Biomol. Chem.*, 2005, **3**, 4392–4394; (*b*) T. Tanaka, H. Tsutsumi, W. Nomura, Y. Tanabe, N. Ohashi, A. Esaka, C. Ochiai, J. Sato, K. Itotani, T. Murakami, K. Ohba, N. Yamamoto, N. Fujii and H. Tamamura, *Org. Biomol. Chem.*, 2008, **6**, 4374–4377; (*c*) T. Tanaka, W. Nomura, T. Narumi, A. Esaka, S. Oishi, N. Ohashi, K. Itotani, B. J. Evans, Z. Wang, S. C. Peiper, N. Fujii and H. Tamamura, *Org. Biomol. Chem.*, 2009, **7**, 3805–3809.

13 H. Tamamura, T. Araki, S. Ueda, Z. Wang, S. Oishi, A. Esaka, J. O. Trent, H. Nakashima, N. Yamamoto, S. C. Peiper, A. Otaka and N. Fujii, *J. Med. Chem.*, 2005, **48**, 3280–3289.

14 S. Ueda, S. Oishi, Z. Wang, T. Araki, H. Tamamura, J. Cluzeau, H. Ohno, S. Kusano, H. Nakashima, J. O. Trent, S. C. Peiper and N. Fujii, *J. Med. Chem.*, 2007, **50**, 192–198.

15 H. Tamamura, K. Hiramatsu, S. Ueda, Z.-X. Wang, S. Kusano, S. Terakubo, J. O. Trent, S. C. Peiper, N. Yamamoto, H. Nakashima, A. Otaka and N. Fujii, *J. Med. Chem.*, 2005, **48**, 380–391.

16 For some recent exapmles of unsubstituted alkene dipeptide isosteres, see: (*a*) S. Oishi, H. Tamamura, M. Yamashita, N. Hamanaka, A. Otaka and N. Fujii, *J. Chem. Soc., Perkin Trans. 1*, 2001, 2445–2451; (*b*) M. M. Vasbinder, E. R. Jarvo and S. J. Miller, *Angew. Chem., Int. Ed.*, 2001, **40**, 2824–2827; (*c*) M. M. Vasbinder and S. J. Miller, *J. Org. Chem.*, 2002, **67**, 6240–6242; (*d*) N. G. Bandur, K. Harms and U. Koert, *Synlett*, 2005, 773–776; (*e*) C. L. Jenkins, M. M. Vasbinder, S. J. Miller and R. T. Raines, *Org. Lett.*, 2005, **7**, 2619–2622; (*f*) D. Wiktelius and K. Luthman, *Org. Biomol. Chem.*, 2007, **5**, 603–605; (*g*) N. G. Bandur, K. Harms and U. Koert, *Synlett*, 2007, 99–102, and references cited therein.

17 For some recent exapmles of fluoroalkene dipeptide isosteres, see: (*a*) A. Otaka, J. Watanabe, A. Yukimasa, Y. Sasaki, H. Watanabe, T. Kinoshita, S. Oishi, H. Tamamura and N. Fujii, *J. Org. Chem.*, 2004, **69**, 1634–1645; (*b*) P. Van der Veken, K. Senten, I. Kertèsz, I. D. Meester, A.-M. Lambeir, M.-B. Maes, S. Scharpè, A. Haemers and K. Augustyns, *J. Med. Chem.*, 2005, **48**, 1768–1780; (*c*) Y. Nakamura, M. Okada, A. Sato, H. Horikawa, M. Koura, A. Saito and T. Taguchi, *Tetrahedron*, 2005, **61**, 5741–5753; (*d*) S. Sano, Y. Kuroda, K. Saito, Y. Ose and Y. Nagao, *Tetrahedron*, 2006, **62**, 11881–11890; (*e*) T. Narumi, A. Niida, K. Tomita, S. Oishi, A. Otaka, H. Ohno and N. Fujii, *Chem. Commun.*, 2006, 4720–4722; (*f*) G. Dutheuil, S. Couve-Bonnaire and X. Pannecoucke, *Angew. Chem., Int. Ed.*, 2007, **46**, 1290–1292; (*g*) T. Narumi, K. Tomita, E. Inokuchi, K. Kobayashi, S. Oishi, H. Ohno and N. Fujii, *Org. Lett.*, 2007, **9**, 3465–3468; (*h*) C. Lamy, J. Hofmann, H. Parrot-Lopez and P. Goekjian, *Tetrahedron Lett.*, 2007, **48**, 6177–6180; (*i*) T. Narumi, K. Tomita, E. Inokuchi, K. Kobayashi, S. Oishi, H. Ohno and N. Fujii, *Tetrahedron*, 2008, **64**, 4332–4346; (*j*) Y. Yamaki, A. Shigenaga, K. Tomita, T. Narumi, N. Fujii and A. Otaka, *J. Org. Chem.*, 2009, **74**, 3272–3277; (*k*) Y. Yamaki, A. Shigenaga, J. Li, Y. Shimohigashi and A. Otaka, *J. Org. Chem.*, 2009, **74**, 3278–3285; (*l*) S. Oishi, H. Kamitani, Y. Kodera, K. Watanabe, K. Kobayashi, T. Narumi, K. Tomita, H. Ohno, T. Naito, E. Kodama, M. Matsuoka and N. Fujii, *Org. Biomol. Chem.*, 2009, **7**, 2872–2877.

18 For some recent examples of tri- or tetrasubstituted alkene isosteres, see: (*a*) S. Oishi, T. Kamano, A. Niida, Y. Odagaki, N. Hamanaka, M. Yamamoto, K. Ajito, H. Tamamura, A. Otaka and N. Fujii, *J. Org. Chem.*, 2002, **67**, 6162–6173; (*b*) S. Oishi, K. Miyamoto, A. Niida, M. Yamamoto, K. Ajito, H. Tamamura, A. Otaka, Y. Kuroda, A. Asai and N. Fujii, *Tetrahedron*, 2006, **62**, 1416–1424; (*c*) J. Xiao, B. Weisblum and P. Wipf, *Org. Lett.*, 2006, **8**, 4731–4734; (*d*) N. Dai, X. J. Wang and F. A. Etzkorn, *J. Am. Chem. Soc.*, 2008, **130**, 5396–5397.

19 (*a*) P. Wipf, T. C. Henninger and S. J. Geib, *J. Org. Chem.*, 1998, **63**, 6088–6089; (*b*) J. Xiao, B. Weisblum and P. Wipf, *J. Am. Chem. Soc.*, 2005, **127**, 5742–5743; (*c*) P. Wipf, J. Xiao and S. J. Geib, *Adv. Synth. Catal.*, 2005, **347**, 1605–1613; (*d*) K. Kobayashi, T. Narumi, S. Oishi, H. Ohno and N. Fujii, *J. Org. Chem.*, 2009, **74**, 4626–4629.

20 S. Couve-Bonnaire, D. Cahard and X. Pannecoucke, *Org. Biomol. Chem.*, 2007, **5**, 1151–1157, and references cited therein.

21 S. Oishi, R. Masuda, B. Evans, S. Ueda, Y. Goto, H. Ohno, A. Hirasawa, G. Tsujimoto, Z. Wang, S. C. Peiper, T. Naito, E. Kodama, M. Matsuoka and N. Fujii, *ChemBioChem*, 2008, **9**, 1154–1158.

22 (*a*) E. Kodama, S. Kohgo, K. Kitano, H. Machida, H. Gatanaga, S. Shigeta and M. Matsuoka, *Antimicrob. Agents Chemother.*, 2001, **45**, 1539–1546; (*b*) Y. Maeda, D. J. Venzon and H. Mitsuya, *J. Infect. Dis.*, 1998, **177**, 1207–1213.

CHEMISTRY
AN ASIAN JOURNAL

DOI: 10.1002/asia.200900465

Binding of Multivalent Anionic Porphyrins to V3 Loop Fragments of an HIV-1 Envelope and Their Antiviral Activity

Kenji Watanabe,[a] Shigeru Negi,[b] Yukio Sugiura,[b] Akiko Kiriyama,[b] Akino Honbo,[b] Katsumi Iga,[b] Eiichi N. Kodama,*[c] Takeshi Naitoh,[d] Masao Matsuoka,[d] and Koji Kano*[a]

Abstract: Interactions of multivalent anionic porphyrins and their iron(III) complexes with cationic peptides, $V3_{Ba\text{-}L}$ and $V3_{IIIB}$, which correspond to those of the V3 loop regions of the gp120 envelope proteins of the HIV-$1_{Ba\text{-}L}$ and HIV-1_{IIIB} strains, respectively, are studied by UV/Vis, circular dichroism, ^{1}H NMR, and EPR spectroscopy, a microcalorimetric titration method, and anti-HIV assays. Tetrakis(3,5-dicarboxylatophenyl)porphyrin (P1), tetrakis[4-(3,5-dicarboxylatophenylmethoxy)phenyl]porphyrin (P2), and their ferric complexes (Fe^{III}P1 and Fe^{III}P2) were used as the multivalent anionic porphyrins. P1 and Fe^{III}P1 formed stable complexes with both V3 peptides (binding constant $K > 10^6\,M^{-1}$) through combined electrostatic and van der Waals interactions. Coordination of the His residues in $V3_{Ba\text{-}L}$ to the iron center of Fe^{III}P1 also played an important role in the complex stabilization. As P2 and Fe^{III}P2 form self-aggregates in aqueous solution even at low concentrations, detailed analysis of their interactions with the V3 peptides could not be performed. To ascertain whether the results obtained in the model system are applicable to a real biological system, anti-HIV-$1_{BA\text{-}L}$ and HIV-1_{IIIB} activity of the porphyrins is examined by multiple nuclear activation of a galactosidase indicator (MAGI) and 3-(4,5-dimethylthiazol-2-yl)-2,5-diphenyltetrazolium bromide (MTT) assays. There is little correlation between chemical analysis and actual anti-HIV activity, and the size rather than the number of the anionic groups of the porphyrin is important for anti-HIV activity. All the porphyrins show high selectivity, low cytotoxicity, and high viral activity. Fe^{III}P1 and Fe^{III}P2 are used for the pharmacokinetic study. Half-lives of these iron porphyrins in serum of male Wistar rats are around 4 to 6 h owing to strong interaction of these porphyrins with serum albumin.

Keywords: antiviral agents · electrostatic interactions · inhibitors · porphyrinoids · proteins

Introduction

Human immunodeficiency virus (HIV) enters T-cells and/or macrophages by binding to the cluster of differentiation 4 (CD4) receptors expressing on the normal cell surfaces. After virus–cell fusion, a single-stranded RNA of HIV is reverse transcribed to a double-stranded DNA, which is then integrated into the host cell genome. A polypeptide is pro-

[a] K. Watanabe, Prof. Dr. K. Kano
Department of Molecular Chemistry and Biochemistry
Faculty of Science and Engineering, Doshisha University
Kyotanabe, Kyoto 610-0321 (Japan)
Fax: (+81) 774-65-6845
E-mail: kkano@mail.doshisha.ac.jp

[b] Dr. S. Negi, Prof. Dr. Y. Sugiura, Dr. A. Kiriyama, A. Honbo, Prof. Dr. K. Iga
Faculty of Pharmaceutical Science
Doshisha Women's College of Liberal Arts
Kyotanabe, Kyoto 610-0395 (Japan)

[c] Dr. E. N. Kodama[+]
Laboratory of Virus Immunology, Institute for Virus Control
Kyoto University
53 Kawaramachi, Shogoin, Sakyo-ku, Kyoto 606-8507 (Japan)

[d] T. Naitoh, Prof. Dr. M. Matsuoka
Laboratory of Virus Immunology, Institute for Virus Control, Kyoto University
53 Kawaramachi, Shogoin, Sakyo-ku, Kyoto 606-8507 (Japan)

[+] Present address:
Division of Emerging Infectious Diseases
Tohoku University School of Medicine
2-1 Seiryo-cho, Aoba-ku, Sendai 980-8575 (Japan)
Fax: (+81) 22-717-8221
E-mail: kodama515@m.tains.tohoku.ac.jp

Supporting information for this article is available on the WWW under http://dx.doi.org/10.1002/asia.200900465.

duced according to the viral genome, followed by proteolytic processing by viral protease. Then the viral proteins and RNA are assembled in the cell membrane, thereby yielding a new virus. The cycle of viral replication causes the destruction of a number of CD4-positive T-cells and/or macrophages.[1]

To suppress HIV proliferation, drugs inhibiting each step of the viral infection are administered.[2] The initial step of viral infection is the binding of the HIV gp120 envelope glycoprotein to the CD4 receptors of T-cells and macrophages.[3] The gp120 glycoprotein possesses a characteristic protruding part called the third variable (V3) loop, a basic, cyclic region that facilitates viral entry by interacting with the CXCR4 or CCR5 coreceptor on the host cell surface.[4] As viral entry is the initial step of the infection, the inhibitors that suppress this step seem to be effective antiviral drugs. Therefore, many drugs that inhibit the viral entry into the host cells have been developed.[5–7] However, very few basic studies have been conducted on the mechanism of action of these drugs.

Abstract in Japanese:

HIV-$1_{Ba\text{-}L}$ および HIV-1_{IIIB} の外部タンパク質である gp120 の V3 ループ部分と同一のアミノ酸配列を有するカチオン性環状ペプチド、$V3_{Ba\text{-}L}$ および $V3_{IIIB}$ を合成し、多価アニオン性ポルフィリンおよびその鉄(III)錯体との相互作用につき研究した。紫外・可視、円二色性、^{1}H NMR および EPR 分光法を研究手段として用いた。tetrakis(3,5-dicarboxylatophenyl)porphyrin (P1)、tetrakis[4-(3,5-dicarboxylato-phenylmethoxy)phenyl]porphyrin (P2) およびこれらの鉄(III)錯体（Fe(III)P1 および Fe(III)P2）を多価アニオン性ポルフィリンとして使用した。P1 および Fe(III)P1 は静電相互作用とファン・デル・ワールス相互作用のの協同効果により、V3 ペプチドと安定な錯体を形成した（$K > 10^6\ M^{-1}$）。$V3_{Ba\text{-}L}$ 中の His 残基が Fe(III)P1 の鉄中心へ配位する効果も、錯体の安定化に重要であった。P2 と Fe(III)P2 とは、低濃度においても水中で自己会合するため、これらのポルフィリン類と V3 ペプチドとの錯形成については詳しく検討できなかった。モデル系の結果を実際の生体系に適応できるかどうかを調べるために、これらのポルフィリン類の抗 HIV 活性を、MAGI 法および MTT 法を用い、HIV-$1_{Ba\text{-}L}$ および HIV-1_{IIIB} 株について検討した。生物学的な検定の結果、薬物の錯形成能と抗 HIV 活性の間には明確な相関性は認められず、薬物に結合したアニオン性置換基の数よりも、薬物の大きさが抗 HIV 活性には重要であることが示唆された。用いた全てのポルフィリンは低い細胞毒性、高い細胞／ウィールス選択性および高い抗ウィルス活性を示した。特に高い抗 HIV 活性を示す Fe(III)P1 と Fe(III)P2 について、薬物動態を調べた。Wister ネズミの血流中でのこれら鉄ポルフィリンの 4〜6 時間という長い滞在時間は、ポルフィリン類の血清アルブミンとの強い相互作用によって説明できる。

Anionic compounds suppress the entry of HIV into CD4 positive cells.[6,7] Among these compounds, anionic porphyrins and phthalocyanines are known to show anti-HIV activity.[7] Most of the previous studies focused on the anti-HIV activity of these anionic macrocycles but no detailed study on their interaction with the proteins related to HIV infection has been reported.

In this study, we examined the interactions between synthetic, cationic V3 loop peptides and multivalent anionic porphyrin free bases and their iron(III) complexes in detail. We also attempted to compare the results obtained from the model system with the anti-HIV activity of these inhibitors. In particular, the effect of the number of anionic groups of the inhibitors, the effect of the sizes of the inhibitors, the driving forces for binding of the inhibitors to the V3 loop peptides, and the effect of Fe^{III} introduced into the porphyrins were intensively studied.

Results and Discussion

Interactions of P1 and Fe^{III}P1 with $V3_{Ba\text{-}L}$

The interactions between the multivalent anionic porphyrins and $V3_{Ba\text{-}L}$ were studied. As the peptide has five basic and two acidic amino acid residues, it possesses three positive net charges at neutral pH. The binding constants (K) for complexation of P1 and Fe^{III}P1 with $V3_{Ba\text{-}L}$ in 20 mM phosphate buffer (pH 7.0) were determined from the UV/Vis spectroscopic titrations (Figure 1). The changes in absorbance of each porphyrin upon the addition of $V3_{Ba\text{-}L}$ were plotted against the concentrations of the peptide. The titration curves were best-fitted with an equation for 1:1 complexation (Figure 1), the determined K values for the P1 and Fe^{III}P1 systems being $(7.6\pm0.5)\times10^6$ and $(4.5\pm0.5)\times10^7\ M^{-1}$, respectively (Table 1). The Job plots (see the Supporting Information) support the formation of 1:1 complexes of the porphyrins and the peptide.

The K values for the P1 and Fe^{III}P1 systems were 25 and 150 times, respectively, higher than that for 5,10,15,20-tetrakis(4-carboxylatophenyl)porphyrin (TCPP; $K=(3.0\pm0.1)\times10^5\ M^{-1}$), which has four anionic groups. An increase in the number of carboxylate groups seems to enhance the binding affinity toward the peptide through electrostatic interaction. In addition, the marked decreases in the K values with increasing ionic strength of the media (Figure 2) support the view that electrostatic interaction is an important force in binding P1 and Fe^{III}P1 to $V3_{Ba\text{-}L}$. The effect of the ionic strength was less effective for the Fe^{III}P1 system than for the P1 system, implying that force(s) other than electrostatic interaction participate in the complexation of Fe^{III}P1. The K values for the Fe^{III}P1–$V3_{Ba\text{-}L}$ system were six times higher than that of the P1–$V3_{Ba\text{-}L}$ system (Table 1), which suggests that the iron center of the porphyrin plays some role in the binding with the peptide.

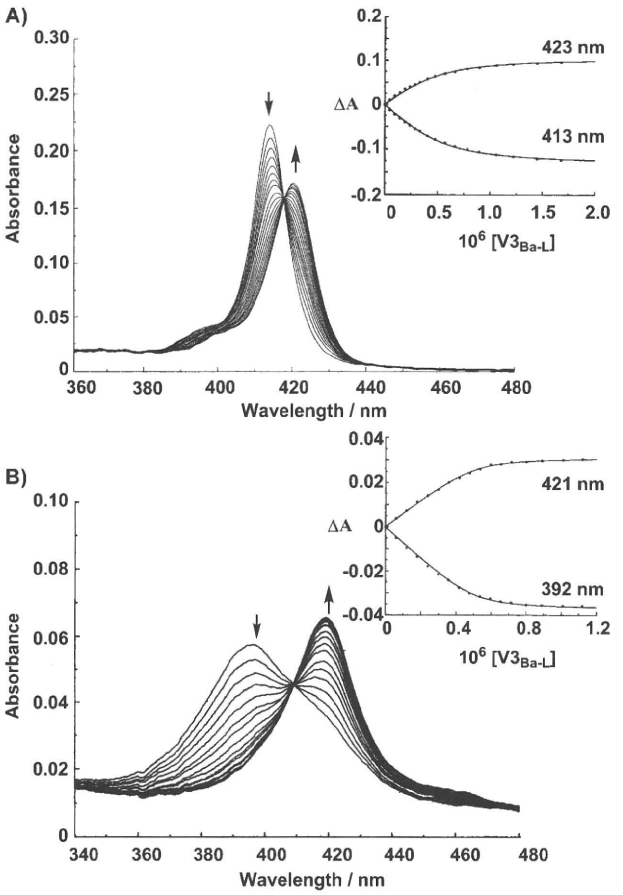

Figure 1. UV/Vis spectral changes of A) P1 (5.0×10^{-7} M) and B) $Fe^{III}P1$ (5.0×10^{-7} M) upon addition of $V3_{Ba\text{-}L}$ in phosphate buffer (0.02 M) at pH 7.0 and 25 °C. Insets are the plots of the absorbance changes versus concentration of $V3_{Ba\text{-}L}$. The solid lines are the best fit of the data to an equation for 1:1 complex formation, thus giving K values.

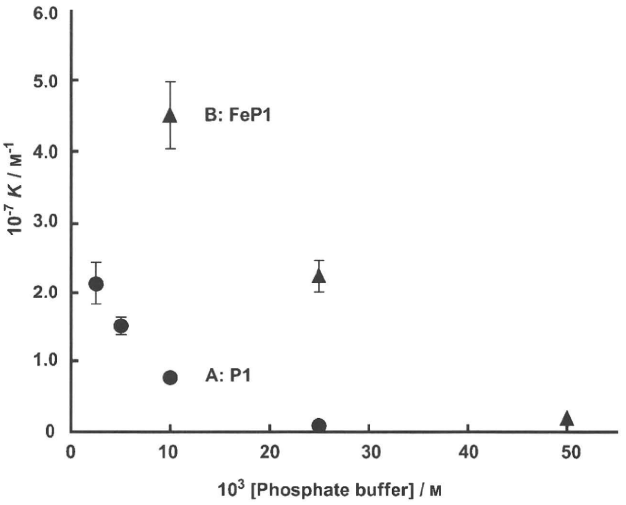

Figure 2. Effects of ionic strength on binding of P1 (●) and $Fe^{III}P1$ (▲) with $V3_{Ba\text{-}L}$ at pH 7.0 and 25 °C. The ionic strength was altered by changing the concentration of the phosphate buffer.

Table 1. Binding constants and thermodynamic parameters for complexation of V3 with P1 and $Fe^{III}P1$ in phosphate buffer (2.0×10^{-2} M) at pH 7.0 and 25 °C.

Porphyrin	Peptide	10^{-7} K [M^{-1}][a]	10^{-7} K [M^{-1}][b]	ΔH^0 [kJ mol^{-1}]	$T\Delta S^0$ [kJ mol^{-1}]	n[c]
P1	$V3_{Ba\text{-}L}$	0.76±0.05	0.47±0.08	−63±1	−25±1	1.0±0.0
	$V3_{Ba\text{-}L}$H13A	0.35±0.02	0.55±0.05	−75±0	−36±0	1.2±0.1
	$V3_{Ba\text{-}L}$H34A	0.58±0.5	0.52±0.12	−71±1	−32±1	0.9±0.1
	$V3_{Ba\text{-}L}$H13A/H34A	0.15±0.2	ND[d]	ND[d]	ND[d]	ND[d]
	$V3_{IIIB}$	11±2	8.5±0.6	−36±1	7.1±1.6	0.9±0.0
$Fe^{III}P1$	$V3_{Ba\text{-}L}$	4.5±0.5	5.2±0.8	−62±3	−18±2	1.0±0.0
	$V3_{Ba\text{-}L}$H13A	0.089±0.03	0.15±0.05	−50±5	−14±5	1.0±0.0
	$V3_{Ba\text{-}L}$H34A	1.4±0.2	0.91±0.15	−56±3	−16±3	1.0±0.0
	$V3_{Ba\text{-}L}$H13A/H34A	0.025±0.001	–	–	–	–
	$V3_{IIIB}$	4.9±1.2	2.6±0.6	−23±2	19±2	0.9±0.0

[a] Binding constants determined by UV/Vis titrations. [b] Binding constants determined by ITC measurements. [c] The n value is the number of sites that corresponds to an inflection point in the titration curve. [d] ND: not determined.

EPR and NMR Spectroscopy

$V3_{Ba\text{-}L}$ comprises 35 amino acid residues including two His residues at positions 13 and 34 (Scheme 1 A). The His residues have the ability to coordinate to $Fe^{III}P1$. To examine the axial coordination, EPR and NMR spectra of the $Fe^{III}P1V3_{Ba\text{-}L}$ complex were measured (Figures 3 and 4). These spectroscopic methods may provide information on the spin state of the $Fe^{III}P1$ complex and its coordination structure.

In the EPR spectrum, the addition of $V3_{Ba\text{-}L}$ to the $Fe^{III}P1$ solution caused disappearance of the signal at $g=6.14$ and appearance of the rhombic signals at $g=2.88$, 2.31, and 2.02 as a result of the low-spin state of the ferric porphyrin (Figure 3B). The EPR spectrum of the $Fe^{III}P1$–$V3_{Ba\text{-}L}$ complex was completely in agreement with that of the bisimidazole complex of $Fe^{III}P1$ [$(Im)_2Fe^{III}P1$] (Figure 3E) as well as with those reported for the bisimidazole complexes of Fe^{III}TPPS (TPPS: 5,10,15,20-tetrakis(4-sulfonatophenyl)porphyrin dianion) and Fe^{III}TPP (TPP: 5,10,15,20-tetraphenylporphyrin dianion).[8,9] These results strongly suggest that the His residues at positions 13 and 34 of $V3_{Ba\text{-}L}$ coordinate to the iron center of $Fe^{III}P1$ when $Fe^{III}P1$ complexes with $V3_{Ba\text{-}L}$.

In general, the β-pyrrole protons of the ferric porphyrins in the high-spin ($S=5/2$) and intermediate-spin states ($S=3/2$) show their ^{1}H NMR spectroscopic signals at approximately $\delta=80$ and −60 ppm at 25 °C, respectively, and therefore the β-pyrrole protons in an admixed intermediate-spin state ($S=5/2$, $3/2$) are observed between $\delta=-60$ and 80 ppm, depending on the contribution of the intermediate-spin state (Int (%)).[10,11] $Fe^{III}P1$ does not form its μ-oxo dimer because of intermolecular electrostatic repulsion between the car-

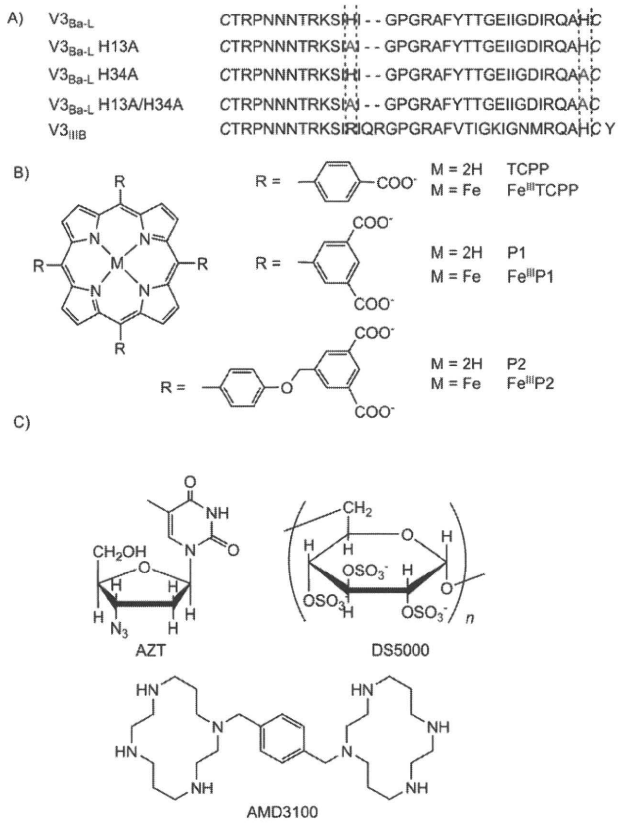

Scheme 1. A) Amino acid sequences of the $V3_{Ba\text{-}L}$, $V3_{Ba\text{-}L}$H13A, $V3_{Ba\text{-}L}$H34A, $V3_{Ba\text{-}L}$H13A/H34A, and $V3_{IIIB}$ peptides. C indicates intramolecular disulfide-bonded cysteine residues. B) Multivalent anionic porphyrins and their iron complexes used in this work. C) Reference compounds used in anti-HIV-1 assays.

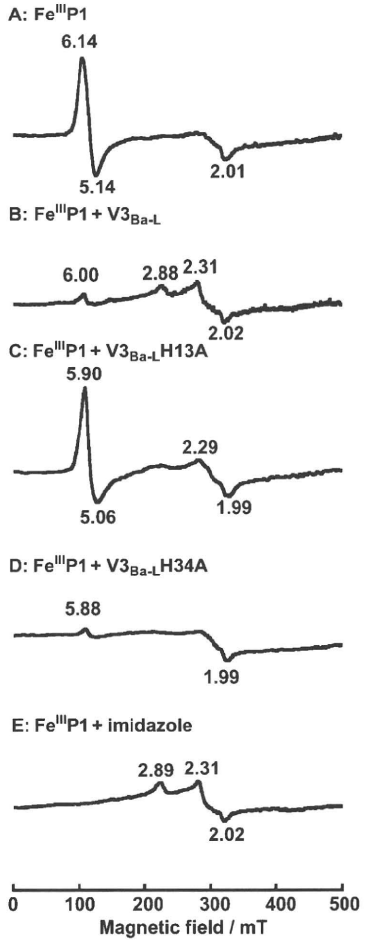

Figure 3. EPR spectra of $Fe^{III}P1$ (4.0×10^{-4} M) in the absence (A) and the presence of B) $V3_{Ba\text{-}L}$, C) $V3_{Ba\text{-}L}$H13A, D) $V3_{Ba\text{-}L}$H34A (6.0×10^{-4} M), and E) imidazole (0.2 M) in 0.02 M phosphate buffer at pH 7.0 and 77 K.

boxylate groups at positions 3 and 5 of the peripheral phenyl groups of the porphyrin.[12] As the pK_a for the equilibrium between the diaqua $[(H_2O)_2Fe^{III}P1]$ and monohydroxo forms $[(OH^-)Fe^{III}P1]$ is 8.0,[12] $Fe^{III}P1$ preferentially exists in the diaqua form in an aqueous solution at pH 7.0. The chemical shift arising from the β-pyrrole protons (δ_{py}) of $[(D_2O)_2Fe^{III}P1]$ was observed at $\delta = 50.4$ ppm (Figure 4A), which is in good agreement with the reported δ_{py} value for $[(D_2O)_2Fe^{III}TPPS]$ in an admixed intermediate-spin state.[13] In the ^{1}H NMR spectrum, the signal arising from the pyrrole protons of $Fe^{III}P1$ shifted to $\delta = -17.4$ ppm upon complexation with $V3_{Ba\text{-}L}$ (Figure 4B), which corresponds to the δ_{py} of $[(Im)_2Fe^{III}P1]$ (Figure 4C). ^{1}H NMR spectroscopy also supports the coordination of the His residues at positions 13 and 34 of $V3_{Ba\text{-}L}$ to the iron center of $Fe^{III}P1$.

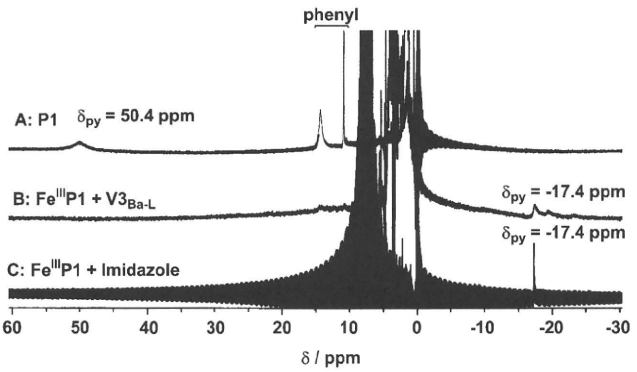

Figure 4. ^{1}H NMR spectra of $Fe^{III}P1$ (2.0×10^{-4} M) in the A) absence and the presence of B) $V3_{Ba\text{-}L}$ (3.0×10^{-4} M) and C) imidazole (0.2 M) in phosphate buffer (2.0×10^{-2} M) at pD 7.0 and 25 °C.

$V3_{Ba\text{-}L}$ Mutants

$V3_{Ba\text{-}L}$ was mutated by substituting the His residues with Ala to confirm the coordination of His to $Fe^{III}P1$. The amino acid sequences of the mutants are shown in Scheme 1A. The mutation of both His residues at positions 13 and 34 ($V3_{Ba\text{-}L}$H13A/H34A) caused a large decrease in the K value for the complexation with $Fe^{III}P1$ (from 4.5×10^7 M^{-1} for $V3_{Ba\text{-}L}$ to 2.5×10^5 M^{-1} for the mutant; Table 1). $V3_{Ba\text{-}L}$H13A, the His residue of which was replaced by Ala at position 13, also showed a significant decrease in the K value

($8.9\times10^5\,M^{-1}$), whereas the replacement at position 34 ($V3_{Ba\text{-}L}$-H34A) showed moderate effect ($K=1.4\times10^7\,M^{-1}$). These results clearly suggest that the His residue at position 13 greatly participates in the stabilization of the $Fe^{III}P1$–$V3_{Ba\text{-}L}$ complex, although the His residue at position 34 assists in the stabilization. The $Fe^{III}P1$–$V3_{Ba\text{-}L}$H34A complex showed an EPR signal at $g=-1.99$ together with a very weak signal at $g=5.88$. Although we could not assign this EPR spectrum, it is clear that the high-spin character of $Fe^{III}P1$ is weakened upon the complexation with $V3_{Ba\text{-}L}$H34A, probably owing to coordination of the His residue at position 13. The EPR spectrum of the $Fe^{III}P1$–$V3_{Ba\text{-}L}$H13A complex (Figure 3C) indicates that the His residue at position 34 barely coordinates to the iron center of $Fe^{III}P1$.

Circular Dichroism

The changes in the secondary structures of $V3_{Ba\text{-}L}$ upon binding with P1 and $Fe^{III}P1$ were studied by means of circular dichroism (CD) spectroscopy. The CD spectra of $V3_{Ba\text{-}L}$ (see the Supporting Information) showed a random coil structure, as previously reported.[14] The negative CD signal of $V3_{Ba\text{-}L}$ at 198 nm decreased and slightly shifted to 199 nm upon addition of P1. Meanwhile, the addition of $Fe^{III}P1$ caused a systematic red-shift of the signal at 198 to 202 nm, thus indicating that the iron of $Fe^{III}P1$ induces a marked structural change of the peptide, which is ascribable to the coordination of the two His residues at positions 13 and 34.

Interactions of P1 and $Fe^{III}P1$ with $V3_{IIIB}$

The interactions of P1 and $Fe^{III}P1$ with $V3_{IIIB}$ were also investigated. $V3_{IIIB}$ has only one His residue at the C-terminal part and contains eight cationic amino acid residues (Lys (K) and Arg (R)). The K values for the complexation of P1 and $Fe^{III}P1$ with $V3_{IIIB}$ were determined to be $(1.1\pm0.2)\times10^8$ and $(4.9\pm1.2)\times10^7\,M^{-1}$, respectively (Table 1). $V3_{IIIB}$ is bound to both P1 and $Fe^{III}P1$ more strongly than $V3_{Ba\text{-}L}$. $V3_{IIIB}$ (net charge = +8) is more basic than $V3_{Ba\text{-}L}$ (net charge = +3). Therefore, electrostatic interactions between the anionic porphyrins and $V3_{IIIB}$ were expected to be much stronger than those for the $V3_{Ba\text{-}L}$ system. Unlike in the case of $V3_{Ba\text{-}L}$, the K value for the complexation of $Fe^{III}P1$ with $V3_{IIIB}$ was significantly smaller than that for P1 (Table 1), thereby suggesting that the iron center of $Fe^{III}P1$ does not participate in the stabilization of the complex because of the absence of a His residue at the middle part of $V3_{IIIB}$. EPR and NMR spectra of the $Fe^{III}P1$–$V3_{IIIB}$ complex could not be measured because of the poor solubility of the complex. Although $V3_{IIIB}$ possesses a His residue at position 35, this His residue at the C-terminal part seems to barely coordinate to $Fe^{III}P1$, as clearly shown in the case of $V3_{Ba\text{-}L}$H13A. The lower K value observed for the $Fe^{III}P1$–$V3_{IIIB}$ system than for the P1–$V3_{IIIB}$ one suggests that electrostatic interaction is the main binding force and the axial ligand of $Fe^{III}P1$, H_2O, seems to interfere with this interaction. The poor solubility of the $V3_{IIIB}$–porphyrin complexes indicates strong interactions of the polycationic peptide and polyanionic porphyrins through coulombic force.

Thermodynamic Parameters

Thermodynamic parameters are very useful in discussing the detailed mechanism of molecular complexation. The interactions of P1 and $Fe^{III}P1$ with the V3 peptides were further studied by means of isothermal titration calorimetry (ITC). Figure 5 shows the typical ITC profiles for the bindings of P1 and $Fe^{III}P1$ with $V3_{Ba\text{-}L}$. The thermodynamic parameters obtained from the ITC measurements are summarized in Table 1.

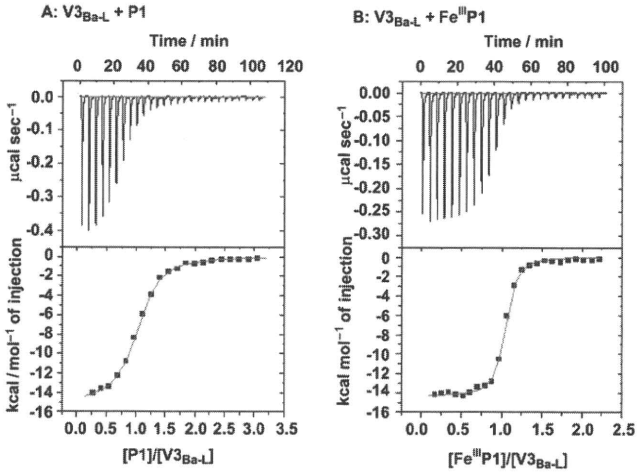

Figure 5. Calorimetric titrations of $V3_{Ba\text{-}L}$ (in cell, 1.4 mL, 5.0×10^{-6} M) with 25 10 µL aliquots of A) P1 (9.9×10^{-5} M) and B) $Fe^{III}P1$ (6.2×10^{-5} M) in phosphate buffer (0.02 M) at pH 7.0 and 25 °C.

The complexation of $V3_{Ba\text{-}L}$ with both P1 and $Fe^{III}P1$ is dominated by the enthalpy terms. Complex formation through electrostatic interaction in aqueous solution is usually driven by a favorable entropy term owing to dehydration from both host and guest.[15] These findings suggest that electrostatic interaction is not the sole binding force for the P1–$V3_{Ba\text{-}L}$ and $Fe^{III}P1$–$V3_{Ba\text{-}L}$ systems. Although coordination of imidazole to iron porphyrins is an enthalpically favorable process,[16] the ΔH^0 ($-62\,kJ\,mol^{-1}$) for the $Fe^{III}P1$–$V3_{Ba\text{-}L}$ system was almost the same as that ($-63\,kJ\,mol^{-1}$) for the P1–$V3_{Ba\text{-}L}$ system. The coordination of the His residue of $V3_{Ba\text{-}L}$ to $Fe^{III}P2$ was not reflected in the ΔH^0 value. Therefore, it is reasonable to assume that van der Waals interaction participates in the complexation and leads to the complicated thermodynamic behavior. Van der Waals interaction in an aqueous solution usually shows a negative ΔH^0 value.[17] The larger K value for $Fe^{III}P1$ than for P1 is ascribable to the larger entropy change. Although the coordination of the two His residues of $V3_{Ba\text{-}L}$ to $Fe^{III}P1$ is entropically unfavorable, dehydration from both the His residues and the iron center upon complexation may cause an increase in ΔS^0. Consequently, it can be concluded that the anionic por-

phyrin is bound to the cationic peptide through combined electrostatic and van der Waals interactions. In addition, the coordination bonds stabilize the $Fe^{III}P1$–$V3_{Ba\text{-}L}$ complex.

The coordination of the His residues to $Fe^{III}P1$ is also supported by the thermodynamic parameters for the complexation of the mutant. The ΔH^0 value for the $Fe^{III}P1$–$V3_{Ba\text{-}L}$ system was (-62 ± 3) kJ mol^{-1}, with an increase to (-50 ± 5) kJ mol^{-1} upon mutation of His at position 13 by Ala ($V3_{Ba\text{-}L}$H13A). As the complexation of $V3_{Ba\text{-}L}$ with P1 is enthalpically less favorable than that of $V3_{Ba\text{-}L}$H13A (Table 1), the enthalpic gain in the $Fe^{III}P1$–$V3_{Ba\text{-}L}$ system is mainly ascribable to the coordination of the two His residues.

Preferential participation of electrostatic interaction in the complexation of P1 and $Fe^{III}P1$ with $V3_{IIIB}$ was clearly reflected in the thermodynamic parameters. Unlike in the case of $V3_{Ba\text{-}L}$, the positive ΔS^0 values were measured for the binding of P1 and $Fe^{III}P1$ to $V3_{IIIB}$ (Table 1). Complexation of multivalent organic ions with oppositely charged ligands in aqueous solution commonly shows positive entropy changes.[15] Extended dehydration from both ions upon association is the origin of the positive ΔS^0. As the complexation of both the anionic porphyrins with $V3_{IIIB}$ having a net charge of +8 is still enthalpically dominated, van der Waals interaction also plays an important role. However, coulombic interaction becomes more obvious in the complexation of $V3_{IIIB}$ than in the case of $V3_{Ba\text{-}L}$.

Interactions of P2 and $Fe^{III}P2$ with $V3_{Ba\text{-}L}$ and $V3_{IIIB}$

According to the X-ray crystallographic data of the V3 loop region of gp120 (PDB code: 2b4c), the sizes of P1 and $Fe^{III}P1$ seemed to be too small to cover the loop peptide totally (see the Supporting Information). The peripheral substituents of the porphyrin were elongated to enlarge the size. We prepared tetrakis[4-(3,5-dicarboxylatophenylmethoxy)phenyl]porphyrin (P2) and its iron(III) complex ($Fe^{III}P2$) (Scheme 1 B) as larger multivalent anionic porphyrins.

UV/Vis spectroscopic titrations for determining the K values for the complexation of P2 and $Fe^{III}P2$ with $V3_{Ba\text{-}L}$ were examined (see the Supporting Information). Unfortunately, however, the self-aggregation behavior of these porphyrins interfered with the attempts. P2 forms stacking-type self-aggregates at $[P2]>1\times10^{-6}$ M (Supporting Information), and $Fe^{III}P2$ forms a μ-oxo dimer (also in the Supporting Information). We applied ITC measurements to estimate the K values. In the ITC measurements, 10 μL aliquots of the 1×10^{-4} M porphyrin in 2×10^{-2} M phosphate buffer in a syringe were successively injected into a 5×10^{-6} M $V3_{Ba\text{-}L}$ solution (1.4 mL) in the same buffer in a cell. P2 was significantly diluted at each injection, thus leading to dissociation of its self-aggregates. The heat of dissociation of the P2 aggregates was cancelled out by the reference titration in which the porphyrin solution in the syringe was injected into the buffer without the peptide. Therefore, the K value and other thermodynamic parameters for the complexation of P2 with $V3_{Ba\text{-}L}$ might be reliable. However, the quality of the ITC titration curve was not satisfactory (Supporting Information) and provided a roughly estimated K value of 2×10^6 M^{-1} for the complexation of P2 with $V3_{Ba\text{-}L}$, which is smaller than the K value for the P1–$V3_{Ba\text{-}L}$ complex (4.7×10^6 M^{-1}). As the energy-minimized structure of P2 (Supporting Information) suggests, it is not necessarily the case that the positions of the carboxylate anionic groups of P2 fit well to the positions of the cationic residues of $V3_{Ba\text{-}L}$ to maximize the interaction between P2 and $V3_{Ba\text{-}L}$.

The $Fe^{III}P2$–$V3_{Ba\text{-}L}$ system showed a characteristic calorimetric titration curve that exhibited two complexation processes (Supporting Information). We could not draw the structures of the $Fe^{III}P2$–$V3_{Ba\text{-}L}$ complexes. In any case, all spectroscopic data indicate that $Fe^{III}P2$ does not bind to the peptide in its μ-oxo-dimer form. In the UV/Vis titration curve, the change in the absorption of $Fe^{III}P2$ was saturated at the equimolar concentration of $V3_{Ba\text{-}L}$, which suggests that the K value of this system is greater than 10^6 M^{-1} if the 1:1 complex is formed.

Owing to the low solubility of the P2–$V3_{IIIB}$ and $Fe^{III}P2$–$V3_{IIIB}$ complexes, detailed studies on the interactions of these enlarged porphyrins and the multivalent peptide could not be performed. Rough estimation by ITC suggests K values in the order of 10^7 M^{-1} on the assumption of the 1:1 stoichiometry. Indeed, the precipitations appeared when an equimolar amount of P2 or $Fe^{III}P2$ was added to the $V3_{IIIB}$ solution, thereby suggesting the formation of a very stable association complex.

Anti-HIV-1 Activity of Porphyrins

Anti-HIV-1 activity of the porphyrins to the HIV-$1_{Ba\text{-}L}$ and HIV-1_{IIIB} strains was determined by multiple nuclear activation of galactosidase indicator cell (MAGI) assay[18] by using HeLa-CD4/CCR5-LTR/β-gal cells expressing both CCR5 and CXCR4. A 3-(4,5-dimethylthiazol-2-yl)-2,5-diphenyltetrazolium bromide (MTT) assay[19] using HIV-1_{IIIB} was also performed. Antiviral activity of a drug is represented by the concentration of the drug at which the viral replication is blocked by 50% (EC_{50}). The results are summarized in Table 2. Zidovudine (AZT, a nucleotide reverse transcrip-

Table 2. Anti-HIV-1 activity (EC_{50} in μM) and cytotoxicity (CC_{50} in μM) of AZT, DS5000, AMD3100, and porphyrins determined by the MAGI and MTT assays.

Inhibitor	EC_{50} [μM][a]		CC_{50} [μM][b]
	HIV-$1_{Ba\text{-}L}$	HIV-1_{IIIB}	
AZT	0.034 ± 0.009	0.023 ± 0.010	>10
DS5000[c]	0.085 ± 0.005	0.062 ± 0.005	>100
AMD3100	>0.2	0.0034 ± 0.0002	>0.2
TCPP	4.7 ± 0.15	2.6 ± 0.23	40 ± 5
Fe^{III}TCPP	0.89 ± 0.21	1.4 ± 0.3	>100
P1	1.9 ± 0.1	1.7 ± 0.6	36 ± 5
$Fe^{III}P1$	0.35 ± 0.03	0.49 ± 0.19	>100
P2	0.19 ± 0.03	0.21 ± 0.05	35 ± 5
$Fe^{III}P2$	0.12 ± 0.02	0.059 ± 0.014	>100

[a] Anti-HIV-1 activity was determined by MAGI assay. [b] Cytotoxicity was determined by the MTT method. [c] The EC_{50} and CC_{50} values of DS5000 are represented as the molar concentrations of a dextran unit.

tase inhibitor), AMD3100 (a CXCR4 antagonist), and DS5000 (a dextran sulfate having an average molecular weight of 5000, an entry inhibitor) (Scheme 1C) were used as the reference drugs.

Over the course of the MAGI assay, we found that the anti-HIV-1 activities of P1 and $Fe^{III}P1$, which have eight carboxylate anionic groups, were higher than those of TCPP and $Fe^{III}TCPP$, respectively, which have four CO_2^- groups. The higher anti-HIV-1 activities of P1 and $Fe^{III}P1$ may be ascribed to the higher ability of these porphyrins to bind to the V3 loops of the viruses. However, in the MTT assay, which needs five days to obtain the results (the drug potency therefore tends to become obscure), P1 and $Fe^{III}P1$ showed a small supremacy of P1 and $Fe^{III}P1$ relative to TCPP and $Fe^{III}TCPP$. Meanwhile, the enlarged porphyrins with eight CO_2^- groups, P2 and $Fe^{III}P2$, definitely showed higher anti-HIV-1 activity than P1 and $Fe^{III}P1$. It seems that P2 and $Fe^{III}P2$ overlap the V3 loops of the HIV-1 strains well, which leads to effective inhibition of the binding of the V3 loop region to the receptors on the target cells. The results in Table 2 clearly indicate that the size of the drug rather than the number of the anionic groups is a very important factor for anti-HIV-1 activity.

Only the $Fe^{III}P1$–HIV-$1_{Ba\text{-}L}$ system has the possibility for coordination of the two His residues in the V3 loop of this virus to the iron of the porphyrin. However, there was no large difference in the anti-HIV-1 activity of $Fe^{III}P1$ between HIV-$1_{Ba\text{-}L}$ and HIV-1_{IIIB}. This means that the coordination of the His residues does not play a significant role in the inhibition of HIV-1 infection, or that the two His residues of HIV-$1_{Ba\text{-}L}$ do not coordinate to $Fe^{III}P1$.

We initially expected a clear correlation between the K values in the model system and the EC_{50} values. If the experimental results were in line with our expectations, we could have obtained a powerful methodology to design anti-HIV-1 drugs. However, the experimental results did not fulfill our expectation, although we found potent activities of P2 and $Fe^{III}P2$.

Effects of Time of Drug Addition and Preincubation

The effects of the time of drug addition on the HIV-1_{IIIB} activity were examined to confirm the mechanism of action of the porphyrins. At $t=0$ h, the HeLa-CD4/CCR5-LTR/β-gal cells were inoculated with the HIV-1_{IIIB}. At the indicated time points, each anti-HIV-1 drug for which the concentration had been adjusted to show 90% inhibition (EC_{90}) was added. Then, the infectivity was determined by counting the blue cells after 48 h culture (see the Experimental Section). The time profile of drug addition of $Fe^{III}P1$ (Figure 6) was almost the same as those for entry inhibitors such as polyanionic DS5000 (gp120-targeted) and polycationic AMD3100 (CXCR4-targeted), thus suggesting that $Fe^{III}P1$ exerts the antiviral activity by blocking viral entry into normal cells.

We examined the effects of preincubation on the HIV-1_{IIIB} infection (Figure 7). A mixture of a drug and the HeLa-CD4/CCR5-LTR/β-gal cells was preincubated for 2 h followed by washing, and then inoculated with HIV-1_{IIIB}. If the drug binds to the target cells, thereby leading to anti-HIV-1 activity, the infection should be suppressed even after preincubation. Meanwhile, if the drug selectively binds to HIV-1, no preincubation effect should be observed. AMD3100 is a CXCR4 antagonist. As AMD3100 bound to CXCR4 of the HeLa cells, this drug showed anti-HIV-1 activity after preincubation. On the other hand, the anionic porphyrins and DS5000 are entry inhibitors, the functions of which are achieved by binding to the V3 loop proteins. As shown in Figure 7, the anionic drugs did not show any antiviral activity after preincubation, thus indicating that these anionic drugs selectively bind to the V3 loops of the HIV-1, which results in the inhibition of HIV-1 entry into the HeLa cells.

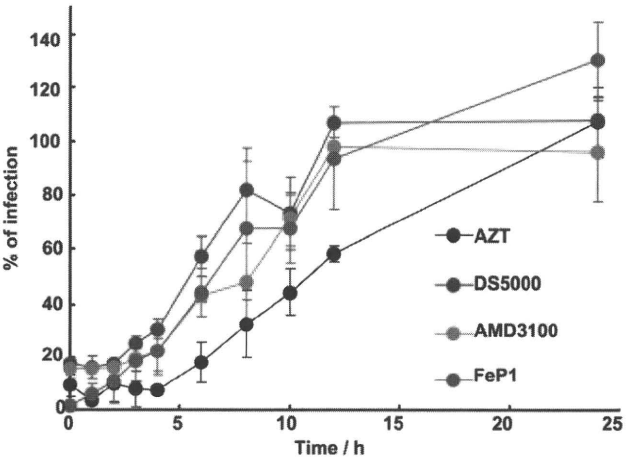

Figure 6. Time of drug-addition profiles for infection of the HIV-1_{IIIB} strain to HeLa-CD4/CCR5-LTR/β-gal cells.

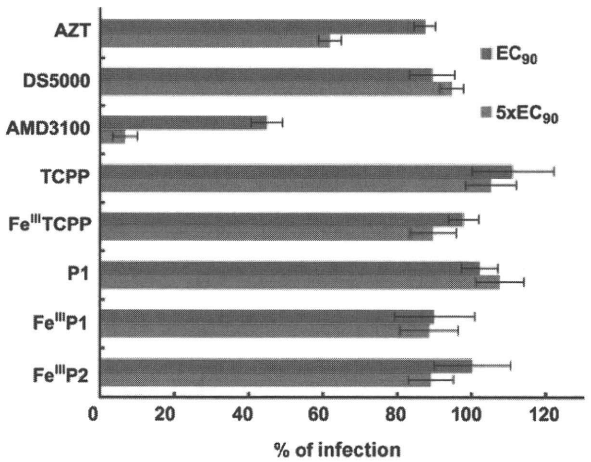

Figure 7. Preincubation effects on the anti-HIV-1 activity. Each drug with the concentrations of EC_{90} and $5\times EC_{90}$ was preincubated with HeLa-CD4/CCR5-LTR/β-gal cells for 2 h and the preincubated samples were washed 5 times with phosphate buffer solution (PBS) before inoculation with the HIV-1_{IIIB} strain.

Cytotoxicity of Porphyrins

The cytotoxicity of a drug is represented by the drug concentration at which the viability of the host cells is suppressed by 50% (CC_{50}). The cytotoxicity of each porphyrin is listed in Table 2. Interestingly, the cytotoxicity of the iron(III) complexes was lower than that of the corresponding porphyrin free bases. A similar effect on the cytotoxicity was reported by Song et al.[7c] The introduction of the iron atom might improve the selectivity of the binding of the porphyrin to the V3 loop region. The low cytotoxicity and high anti-HIV-1 activity of these iron(III) porphyrins are a large benefit to the usage of these metal complexes.

Pharmacokinetics

$Fe^{III}P1$ and $Fe^{III}P2$, which show high antiviral activities, were selected for a pharmacokinetic study to confirm whether these compounds can be applied to anti-HIV-1 drugs. $Fe^{III}P1$ and $Fe^{III}P2$ were dissolved into polyethylene glycol (PEG400; average molecular weight of 400) and intravenously (iv) infused into the right femoral vein of male Wistar rats after anesthetizing with urethane. Blood samples were collected from the jugular vein, and the plasma concentrations of the drugs were measured by the HPLC method. Plasma concentration–time curves of the drugs in rat plasma after the infusions are shown in Figure 8. The concentrations of $Fe^{III}P1$ and $Fe^{III}P2$ reached the maximum at 10 and 30 min, respectively, after the infusions. Long elimination half-lives of $Fe^{III}P1$ (229 min) and $Fe^{III}P2$ (384 min) were observed. The long residence times of these iron porphyrins seem to be ascribable to strong binding of the porphyrins to serum albumin (see the Supporting Information). The difference in the elimination half-life times between $Fe^{III}P1$ and $Fe^{III}P2$ can be interpreted in terms of the difference in their binding affinities for serum albumin.

Interestingly, $Fe^{III}P1$ administrated intraduodenally (id) moved into the bloodstream slightly, although no movement of $Fe^{III}P2$ was observed. The bioavailability (BA) was calculated from the area under the curves, AUC_{iv} and AUC_{id}, which were normalized by the dose according to the following equation: $BA = AUC_{id}/AUC_{iv}$. The BA of $Fe^{III}P1$ at 15.0 and 30.0 mg kg^{-1} doses were 1.49 and 1.09%, respectively. $Fe^{III}P2$, however, was definitely not absorbed by the gastrointestinal tract. This might be ascribed to its large molecular weight. As the absorption of water-soluble iron(III) porphyrins into the bloodstream is very low, we have to develop drug carriers that assist the absorption of hydrophilic drugs such as $Fe^{III}P1$ and $Fe^{III}P2$ for practical application of these porphyrins as anti-HIV drugs.

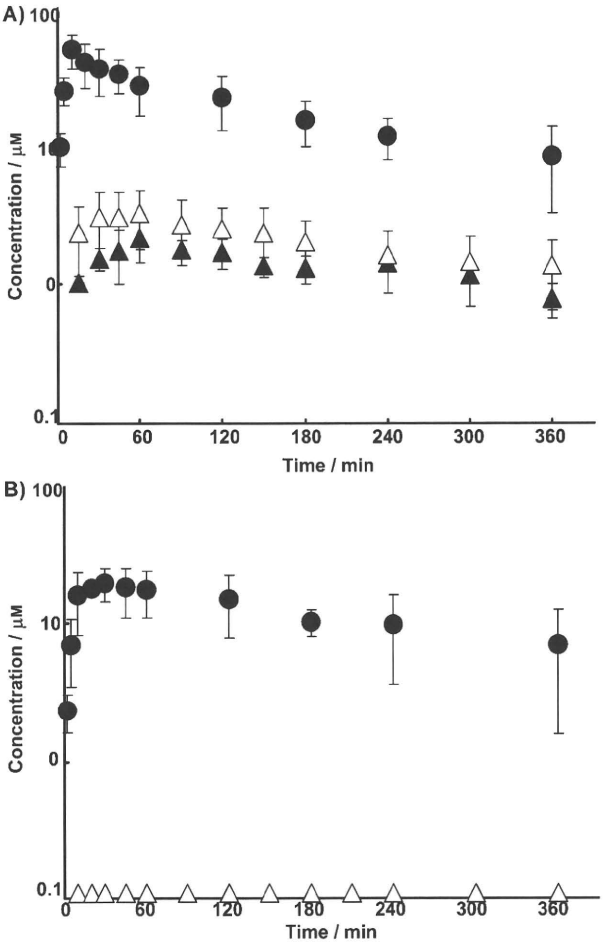

Figure 8. Plasma concentration–time profiles of A) $Fe^{III}P1$ and B) $Fe^{III}P2$ after intravenous infusion (●, 2 mg kg^{-1}) and intraduodenal administration (▲, 15 mg kg^{-1}; △, 30 mg kg^{-1}) to the rats.

Experimental Section

Instruments

UV/Vis and CD spectra were measured using a Shimadzu UV-2100 spectrophotometer and a Jasco J820 spectropolarimeter, respectively. EPR and NMR spectra were recorded using a Jasco JES-TE200 system and a Bruker Biospin AVANCE system, respectively. MALDI-TOF MS and ESI-TOF MS were performed by using an Applied Biosystem Voyager-DE STR system and a JEOL JMS-T-100CS system, respectively. A Horiba F-52 pH meter was applied to measure the pH of the solutions.

Reagents

Bovine serum albumin (BSA) was purchased from Sigma (St. Louis, MO; Lot No. 082K1150) and used as received. AZT and DS5000 were purchased from Sigma and used as received. Water was purified by using Millipore Simpak 1.

Peptides

The amino acid sequences of the peptides used in this study are shown in Scheme 1 A. $V3_{Ba\text{-}L}$ and $V3_{IIIB}$, the amino acid sequences of which corresponded to those of the V3 loop regions of strains HIV-$1_{Ba\text{-}L}$ and HIV-1_{IIIB}, respectively, and alanine mutants of $V3_{Ba\text{-}L}$ ($V3_{Ba\text{-}L}$H13A, $V3_{Ba\text{-}L}$H34A, and $V3_{Ba\text{-}L}$H13A/H34A) were chemically synthesized by 9-fluorenylmethyloxycarbonyl (Fmoc) solid-phase peptide synthesis with TGS-RAM resin (Shimadzu, Kyoto, Japan) by using a Shimadzu PSSM-8 peptide synthesizer. Fmoc deprotection was performed with 30% (v/v) piperidine in DMF, and coupling reactions were carried out with a mixture of Fmoc-amino acid (10 equiv), *O*-(7-azabenzotriazol-1-yl)-1,1,3,3-tetramethyluronium hexafluorophosphate (HATU; 1.2 equiv), 1-hydroxy-7-azabenzotriazole (HOAt; 1.2 equiv), and *N*,*N*-diisopropylethylamine (2.4 equiv) in DMF. A tyrosine residue was inserted into the C-terminal

of $V3_{IIIB}$ as a marker for determining its concentration. After the coupling reactions, the peptide was cut off from the resin by using a mixture of trifluoroacetic acid (TFA), 1,2-ethanediol, thioanisole, triisopropylsilane, and water (86:5:5:1.5:2.5% (v/v)) and precipitated from diethyl ether. The peptide was purified by using a reverse-phase HPLC (RP-HPLC) system (Hitachi ELITE LaChrom) equipped with a Nacalai Tesque COSMOSIL 5C18-AR-II column. The target proteins were eluted with a gradient of CH_3CN/H_2O containing 0.1% (v/v) TFA (1:4 to 2:3). The purified peptides were dissolved in 50 mM tris(hydroxymethyl)aminomethane (Tris)-HCl buffer (pH 8.0, [peptide] $\approx$ 60 μM) and the resulting solution was stirred under air bubbling for 24 h. The 5,5′-dithiobis(2-nitrobenzoic acid) (DTNB) assay was applied to confirm the conversion of the thiol groups to the disulfide bond. The peptide solutions were then neutralized with a 6 M aqueous NaOH solution to pH 7.0, and concentrated under reduced pressure followed by lipophilization. The peptides were further purified by reversed-phase (RP) HPLC using the same manner as the first purification step. The fidelity of the products was checked by MALDI-TOF MS: *m/z* calcd for $V3_{Ba\text{-}L}$: 3895.4; found: 3894.9; calcd for $V3_{Ba\text{-}L}H13A$: 3829.4; found: 3828.9; calcd for $V3_{Ba\text{-}L}H34A$: 3829.4; found: 3828.8; calcd for $V3_{Ba\text{-}L}H13A/H34A$: 3765.3; found: 3765.4; calcd for $V3_{IIIB}$: 4212.8; found: 4212.9.

Anionic Porphyrins

P1[20] and Fe^{III}P1[12] were synthesized according to the procedures described in the literature. TCPP and Fe^{III}TCPP were purchased from Tokyo Chem. Ind. Co. (Tokyo, Japan) and Frontier Scientific Inc. (Logan, UT), respectively, and used without further purifications.

P2 was synthesized by the hydrolysis of tetrakis[4-(3,5-diethoxycarbonylphenylmethoxy)phenyl]porphyrin (200 mg)[21] in a mixed solution of 3 M aqueous KOH solution (20 mL) and THF (120 mL). The solution was heated at reflux for 12 h under protection from light. After the reaction, the organic solvents were evaporated, and the aqueous residues were washed with dichloromethane. The aqueous phase was then acidified with HCl and the P2 precipitates were collected by filtration. Yield (156 mg, 90%); ^{1}H NMR (500 MHz, [D_6]DMSO, 25 °C, TMS): $\delta = -2.89$ (s, 2H; NH), 5.59 (s, 8H; OCH_2), 7.51 (d, ^3J(H,H) = 8.8 Hz, 8H; phenyl), 8.17 (d, ^3J(H,H) = 8.8 Hz, 8H; phenyl), 8.44 (d, ^3J(H,H) = 1.6 Hz, 8H; diethylcarboxyphenyl), 8.53 (d, ^3J(H,H) = 1.6 Hz, 4H; diethylcarboxyphenyl), 8.87 (s, 8H; β-pyrrole), 13.40 ppm (s, 8H; carboxy); MS (ESI-TOF): *m/z* (%):1391.3 [M+H^+]; elemental analysis: calcd (%) for $C_{80}H_{54}N_4O_2{\cdot}2HCl{\cdot}3H_2O$ (1518.3): C 63.29, H 4.12, N 3.69; found: C 63.00, H 4.11, N 3.62. Fe^{III}P2 was prepared according to the procedures described in a literature.[21] The purities of P2 and Fe^{III}P2 were checked by HPLC (see the Supporting Information).

Cells and Viruses

MT-4 cells were grown in RPMI-1640 medium supplemented with fetal calf serum (FCS; 10%), L-glutamine (2 mM), penicillin (100 U mL^{-1}), and streptomycin (50 μg mL^{-1}). HeLa-CD4/CCR5-LTR/β-gal cells[22] were kindly provided by Dr. J. Overbaugh through the AIDS Research and Reference Reagent Program, Division of AIDS, National Institute of Allergy and Infectious Disease (NIAID, Bethesda, MD) and maintained in Dulbecco's Modified Eagle Medium (DMEM) supplemented with FCS (10%), hygromycin B (200 μg mL^{-1}), puromycin (10 μg mL^{-1}), and geneticin (200 μg mL^{-1}).

Two laboratory strains, $HIV\text{-}1_{IIIB}$ and $HIV\text{-}1_{Ba\text{-}L}$, were used as CXCR4 and CCR5 tropic HIVs, respectively.

Anti-HIV-1 and Cytotoxicity Assays

The anti-HIV-1 activity of the drugs was determined by MAGI[18] and MTT colorimetric assays.[19] The cytotoxicity of the drugs was determined by the MTT method.

For the MAGI assay, HeLa-CD4/CCR5-LTR/β-gal cells (10^4 cells well^{-1}) were plated on 96-well flat microtiter culture plates. On the following day, the cells were inoculated with the HIV-1 clones (60 MAGI units per well, thereby giving 60 blue cells after 48 h of incubation) and cultured in the presence of various concentrations of the drugs in fresh medium. At 48 h after viral exposure, all the blue cells stained with X-Gal were counted in each well. The activity of the test compounds was determined as the EC_{50}.

The MAGI assay was also employed in drug-addition experiments. The concentrations of the tested inhibitors were fixed at their EC_{90}. At the indicated time points, the compounds were added to $HIV\text{-}1_{LAI}$-exposed MAGI cells. The infected cells in each well were counted as already described.

For the MTT assay, culture medium (100 μL) containing an appropriate concentration of the drug was added to duplicate wells of flat-bottom 96-well plates, and serial tenfold dilutions were made directly in the plates. The MT-4 cells (10^4 cells per well) were mixed with $HIV\text{-}1_{IIIB}$ at a titer of 100 times the 50% tissue culture infectious dose (100 $TCID_{50}$) in the presence and absence of various concentrations of the drug in the plate. After 5 d, the MTT solution (20 μL; 7.5 mg mL^{-1} in PBS) was added to each well of the plates, and the plates were then incubated at 37 °C for 3 h. After incubation, the medium (120 μL) was removed from each well. To dissolve the formazan crystals, isopropanol (100 μL) that contained Triton X-100 (4%) and concentrated HCl (0.4%) was added to each and mixed. After confirming microscopically that the formazan crystals were completely dissolved, the absorbance of each well was measured by using a plate reader (Model 3550, Bio-Rad Laboratories, San Jose, CA) at a wavelength of 595 nm. The CC_{50} of the compound was defined as the concentration that reduced the absorbance of mock-infected cells by 50% of the control.

The MAGI assay was employed for studying the preincubation effect. To evaluate the interaction of each drug with the target cells, the test drug at concentrations of EC_{90} or $5 \times EC_{90}$ were added to HeLa-CD4/CCR5-LTR/β-gal cells in 96-well plates and incubated at 37 °C for 2 h. The cells were washed 5 times with culture media (200 μL) and then inoculated with 60 MAGI units per well of $HIV\text{-}1_{IIIB}$. After 48 h, the stained (infected) cells were counted as previously described.

Pharmacokinetics

Fe^{III}P1 and Fe^{III}P2 were dissolved into PEG400 (0.4 mL) and intravenously infused into the right femoral vein of male Wistar rats for 10 min under urethane (1.0 g kg^{-1} rat body weight) anesthesia. The administered dose was 2 mg kg^{-1} per rat body weight. Blood samples were obtained from the jugular vein, and the plasma concentrations of the drugs were measured by the HPLC method. Cosmosil $5C_{18}$-MS-II (Nacalai Tesque, Kyoto Japan) was used as the analytical column and maintained at 40 °C by using a Shimadzu CTO-20A column oven (Shimadzu, Kyoto, Japan). The composition of the mobile phase was 50:50 (v/v) of methanol and phosphate buffer (50 mM, pH 7.6).

In the intraduodenal dosing study, a midline incision was made and Fe^{III}P1 or Fe^{III}P2 was injected into the rat duodenum through the stomach wall. The concentration of the porphyrin in the bloodstream was determined by the same method as already described.

All animal experiments were performed in accordance with the Guidelines for Animal Experiments of Doshisha Women's College of Liberal Arts.

Acknowledgements

This work was supported by "Creating Research Center for Advanced Molecular Biochemistry", Strategic Development of Research Infrastructure for Private Universities, the Ministry of Education, Culture, Sports, Science and Technology, Japan.

[1] P. R. Clapham, R. A. Weiss, M. Stevenson in *Textbook of AIDS Medicine* (Eds.: T. C. Merigan, Jr., J. G. Bartlett, D. Bolognesi), Lippincott Williams&Wilkins, Baltimore, **1999**, pp. 13–48.

[2] For reviews: a) E. De Clercq, *Nat. Rev. Drug Discovery* **2007**, *6*, 1001–1018; b) C. Flexner, *Nat. Rev. Drug Discovery* **2007**, *6*, 959–966; c) H. Mitsuya, J. Erickson in *Textbook of AIDS Medicine*

(Eds.: T. C. Merigan, Jr., J. G. Bartlett, D. Bolognesi), Lippincott Williams&Wilkins, Baltimore, **1999**, pp. 751–780.

[3] a) R. Wyatt, J. Sodroski, *Science* **1998**, *280*, 1884–1888; b) D. Klatzmann, E. Champagne, S. Chamaret, J. Gruest, D. Guetard, T. Hercend, J.-C. Gluckman, L. Montagnier, *Nature* **1984**, *312*, 767–768; c) J. S. McDougal, M. S. Kennedy, J. M. Sligh, S. P. Cort, A. Mawle, J. K. Nicholson, *Science* **1986**, *231*, 382–385.

[4] a) O. Hartley, P. J. Klasse, Q. J. Sattentau, J. P. Moore, *AIDS Res. Hum. Retroviruses* **2005**, *21*, 171–189; b) C.-C. Huang, M. Tang, M.-Y. Zhang, S. Majeed, E. Montabana, R. L. Stanfield, D. S. Dimitrov, B. Korber, J. Sodroski, I. A. Wilson, R. Wyatt, P. D. Kwong, *Science* **2005**, *310*, 1025–1028; c) H. Choe, M. Farzan, Y. Sun, N. Sullivan, B. Rollins, P. D. Ponath, L. Wu, C. R. Mackay, G. LaRosa, W. Newman, N. Gerard, C. Gerard, J. Sodroski, *Cell* **1996**, *85*, 1135–1148; d) I. Mondor, M. Moulard, S. Ugolini, P.-J. Klasse, J. Hoxie, A. Amara, T. Delaunay, R. Wyatt, J. Sodroski, Q. J. Sattentau, *Virology* **1998**, *248*, 394–405.

[5] For recent reviews: a) E. De Clercq, *Int. J. Antimicrob. Agents* **2009**, *33*, 307–320; b) K. Qian, S. L. Morris-Natschke, K.-H. Lee, *Med. Res. Rev.* **2009**, *29*, 369–393; c) S. Rusconi, A. Scozzafava, A. Mastrolorezo, C. T. Supuran, *Curr. Top. Med. Chem.* **2007**, *7*, 1273–1289.

[6] a) D. J. Clanton, R. A. Moran, J. B. McMahon, O. S. Weislow, R. W. Buckheit, Jr., M. G. Hollingshead, V. Ciminale, B. K. Felber, G. N. Pavlakis, J. P. Bader, *J. Acquired Immune Defic. Syndr.* **1992**, *5*, 771–781; b) P. Mohan, M. F. Wong, S. Verma, P. P. Huang, A. Wickramasinghe, M. Baba, *J. Med. Chem.* **1993**, *36*, 1996–2003; c) S. M. Halliday, C. Lachman-Smith, J. P. Bader, W. G. Rice, D. J. Clanton, L. H. Zalkow, R. W. Buckheit, Jr., *Antiviral Res.* **1996**, *33*, 41–53; d) M. Ono, Y, Wada, Y. Wu, R. Nemori, Y. Jinbo, H. Wang, K. M. Lo, N. Yamaguchi, B. Brunkhorst, H. Otomo, J. Wesolowski, J. C. Way, I. Itoh, S. Gillies, L. B. Chen, *Nat. Biotechnol.* **1997**, *15*, 343–348.

[7] a) A. K. Debnath, S. Jiang, N. Strick, K. Lin, P. Haberfield, A. R. Neurath, *J. Med. Chem.* **1994**, *37*, 1099–1108; b) R. Neurath, N. Strick, A. K. Debnath, *J. Mol. Recognit.* **1995**, *8*, 345–357; c) R. Song, M. Witvrouw, D. Schols, A. Robert, J. Balzarini, E. De Clercq, J. Bernadou, B. Meunier, *Antiviral Chem. Chemother.* **1997**, *8*, 85–97; d) A. N. Vzorov, D. W. Dixon, J. S. Trommel, L. G. Marzilli, R. W. Compans, *Antimicrob. Agents Chemother.* **2002**, *46*, 3917–3925; e) A. N. Vzorov, J. Bozja, D. W. Dixon, L. G. Marzilli, R. W. Compans, *Antiviral Res.* **2007**, *73*, 60–68.

[8] V. E. Yushmanov, H. Imasato, T. T. Tominaga, M. Tabak, *J. Inorg. Biochem.* **1996**, *61*, 233–250.

[9] F. A. Walker, B. H. Huynh, W. R. Scheidt, S. R. Osvath, *J. Am. Chem. Soc.* **1986**, *108*, 5288–5297.

[10] A. Ikezaki, M. Nakamura, *Inorg. Chem.* **2002**, *41*, 6225–6236.

[11] a) C. A. Reed, F. Guiset, *J. Am. Chem. Soc.* **1996**, *118*, 3281–3282; b) D. R. Evans, C. A. Reed, *J. Am. Chem. Soc.* **2000**, *122*, 4660–4667.

[12] K. Kano, R. Nishiyabu, T. Yamazaki, I. Yamazaki, *J. Am. Chem. Soc.* **2003**, *125*, 10625–10634.

[13] M. A. Ivanca, A. G. Lappin, W. R. Scheidt, *Inorg. Chem.* **1991**, *30*, 711–718.

[14] W. F. Vranken, M. Budesinsky, F. Fant, K. Boulez, F. A. M. Borremans, *FEBS Lett.* **1995**, *374*, 117–121.

[15] a) K. Kano, Y. Kitae, Y. Shimofuri, N. Tanaka, Y. Mineta, *Chem. Eur. J.* **2000**, *6*, 2705–2713; b) K. Kano, Y. Ishida, *Angew. Chem.* **2007**, *119*, 741–744; *Angew. Chem. Int. Ed.* **2007**, *46*, 727–730; c) K. Kano, Y. Ishida, K. Kitagawa, M. Yasuda, M. Watanabe, *Chem. Asian J.* **2007**, *2*, 1305–1313.

[16] a) R. F. Pasternack, B. S. Gillies, J. R. Stahlbush, *J. Am. Chem. Soc.* **1978**, *100*, 2613–2619; b) C. B. Perry, T. Chick, A. Ntlokwana, G. Davies, H. M. Marques, *J. Chem. Soc. Dalton Trans.* **2002**, 449–457.

[17] a) D. B. Smithrud, F. Diederich, *J. Am. Chem. Soc.* **1990**, *112*, 339–343; b) K. Kano, K. Fukuda, H. Wakami, R. Nishiyabu, R. F. Pasternack, *J. Am. Chem. Soc.* **2000**, *122*, 7494–7502.

[18] D. Nameki, E. Kodama, M. Ikeuchi, N. Mabuchi, A. Otaka, H. Tamamura, M. Ohno, N. Fujii, M. Matsuoka, *J. Virol.* **2005**, *79*, 764–770.

[19] a) T. Mosmann, *J. Immunol. Methods* **1983**, *65*, 55–63; b) E. Kodama, S. Kohgo, K. Kitano, H. Machida, H. Gatanaga, S. Shigeta, M. Matsuoka, H. Ohrui, H. Mitsuya, *Antimicrob. Agents Chemother.* **2001**, *45*, 1539–1546; c) K. Kajiwara, E. Kodama, M. Matsuoka, *Antiviral Chem. Chemother.* **2006**, *17*, 215–223.

[20] W. Fudickar, J. Zimmermann, L. Ruhlmann, J. Schneider, B. Roder, U. Siggel, J. H. Fuhrhop, *J. Am. Chem. Soc.* **1999**, *121*, 9539–9545.

[21] K. Kano, Y. Ishida, *Chem. Asian J.* **2008**, *3*, 678–686.

[22] B. Chackerian, E. M. Long, P. A. Luciw, J. Overbaugh, *J. Virol.* **1997**, *71*, 3932–3939.

Received: October 19, 2009
Published online: January 28, 2010

Antiviral Chemistry & Chemotherapy 2010 20:239–248 (doi: 10.3851/IMP1597)

Original article

Procyanidin B1 purified from *Cinnamomi cortex* suppresses hepatitis C virus replication

Shenwei Li[1], Eiichi N Kodama[1], Yuuki Inoue[2], Hideki Tani[3], Yoshiharu Matsuura[3], Jing Zhang[4], Takashi Tanaka[5] and Toshio Hattori[1]*

[1]Division of Emerging Infectious Diseases, Department of Internal Medicine, Tohoku University, Sendai, Japan
[2]Department of Microbiology and Immunology, Tohoku University, Sendai, Japan
[3]Department of Molecular Virology, Research Institute for Microbial Diseases, Osaka University, Osaka, Japan
[4]Research and Development Center, FUSO Pharmaceutical Industries, Ltd, Osaka, Japan
[5]Graduate School of Biomedical Sciences, Nagasaki University, Nagasaki, Japan

*Corresponding author: e-mail: kodama515@med.tohoku.ac.jp

Background: A combination of pegylated interferon and ribavirin is the current standard therapy for hepatitis C virus (HCV) infection, but this combination provides relatively low efficacy, especially in some patients with HCV genotype 1 infection; therefore, the development of novel therapeutic agents is required for further improvement in the treatment of chronic HCV infection.
Methods: HCV pseudotype and subgenomic replicon assays were used in this study. The interaction of compounds with HCV receptors was examined using flow cytometry. Intracellular RNA levels were determined by semi-quantitative reverse transcriptase PCR.
Results: Procyanidin B1 (PB1), a dimer of (-)-epicatechin and (+)-catechin, purified from *Cinnamomi cortex*, inhibits infection by vesicular stomatitis virus and HCV pseudotype virus in Huh-7 cells, with 50% effective concentrations of 29 and 15 μM, respectively. No inhibitory effects were observed in each component of PB1. We found that PB1 does not interfere with viral entry or receptor expression, but inhibits HCV RNA synthesis in a dose-dependent manner.
Conclusions: These results indicate that PB1 suppresses HCV RNA synthesis, possibly as a HCV RNA polymerase inhibitor. Our results might contribute towards the development of more effective inhibitors for HCV infection from natural plants.

Introduction

Hepatitis C virus (HCV) is an enveloped, single-stranded, positive RNA virus and is the only member of the *Hepacivirus* genus of the *Flaviviridae*. HCV infection, affecting approximately 170 million people worldwide, leads to chronic hepatitis, liver cirrhosis and, ultimately, hepatocellular carcinoma [1]. Currently, no protective vaccine against HCV is available and treatment is mainly restricted to a combination of pegylated interferon (PEG-IFN) and ribavirin [2]. The sustained virological response (SVR) of treatment is dependent on the HCV genotype. For HCV genotype 1, the SVR rates are between 44% and 56% at 48 weeks of the therapy, whereas for genotypes 2 and 3, they are between 61% and 76% at only 24 weeks of therapy [3,4], indicating that the current standard therapy is insufficient for HCV-infected patients, especially for patients infected with HCV genotype 1. Moreover, the regimen has poor tolerability, especially for long-term treatment – up to 48 weeks – often leading to dose reductions or treatment interruptions [3]. In addition, recombinant IFN is expensive and requires injections for administration. Considering the limited efficacy, serious side effects and high cost, the development of novel, potent and tolerable antiviral agents is urgently needed.

To date, many specifically targeted antiviral compounds designed to inhibit HCV serine protease or RNA-dependent RNA polymerase have been examined in clinical trials, such as telaprevir (an HCV protease inhibitor [5]) and filibuvir (a non-nucleoside HCV polymerase inhibitor [6]) and many other promising compounds. Telaprevir monotherapy for 2 weeks resulted in a reduction of up to 5 $\log_{10}$ IU/ml in plasma HCV RNA levels in patients infected with HCV genotype 1 in Phase Ib trials

[5]. Currently, telaprevir is in a Phase III clinical trial. Filibuvir allosterically inhibits HCV RNA polymerase through binding at the 'thumb 2' site of RNA polymerase. Filibuvir has been recently tested in a Phase II clinical evaluation in patients with HCV genotype 1. Up to 75% of patients treated with filibuvir plus PEG-IFN/ribavirin had undetectable viral load at week 4.

In our previous study, procyanidins, a class of flavanols, purified from *Cinnamomi cortex* inhibited severe acute respiratory syndrome coronavirus (SARS–CoV) replication *in vitro* [7]. We examined the effects of procyanidin B1 (PB1) on the entire HCV replication process using two HCV assays (HCV pseudotype and subgenomic replicon systems) and further studied the mechanisms of action of PB1 on HCV replication. Our results might contribute towards the development of novel effective compounds from natural plants for HCV therapy.

Methods

Cells and reagents

Human hepatocarcinoma Huh-7 cells were maintained in Dulbecco's modified Eagle's medium supplemented with 10% heat-inactivated fetal bovine serum (Gibco BRL, Grand Island, NY, USA), 100 U/ml penicillin G, 100 μg/ml streptomycin and L-glutamine (Gibco BRL). PB1 was purified from *Cinnamomi cortex* as described previously [8] and its structure is shown in Figure 1A. Chlorpromazine, methyl-β-cyclodextrin (MβCD), ribavirin, (-)-epicatechin and (+)-catechin were purchased from Sigma (St Louis, MO, USA), dissolved in water and filtrated.

Pseudotype virus infection assays

We previously reported the generation of vesicular stomatitis virus (VSV)-based pseudotype viruses bearing HCV envelope proteins E1 and E2 (HCVpv) or VSV glycoprotein (VSVpv), which exhibited high infectivity in Huh-7 cells, as shown in Figure 1B [9]. Briefly, 293T cells were transfected with an expression plasmid encoding the HCV E1 and E2 genes of Con1 strains (HCV genotype 1b) and then infected with a VSV envelope protein G (VSV-G)-complemented pseudotype virus (VSVΔG/GFP-G). The HCVpv released from 293T cells were able to infect Huh-7 cells but were unable to produce infectious progeny virus. VSVpv was produced in 293T cells transfected with pVSVΔG/GFP and pCAG-VSV-G and used as controls. The green fluorescent protein (GFP) in each pseudotype virus was replaced by a firefly luciferase gene. Prior to HCVpv or VSVpv infection, Huh-7 cells were incubated with PB1 at 37°C for 1 h. After 48 h of the pseudotype virus infection, cells were harvested, lysed and subjected to luciferase assays using a Mithras LB940 Reader (Berthold Technologies, Bad Wildbad, Germany). The 50% effective concentration (EC_{50}) was defined as the concentration that reduced viral replication by 50%.

Entry assays based on intracellular p24 gag

Chlorpromazine, a cationic amphiphilic compound, inhibits clathrin-dependent endocytosis by preventing the assembly of clathrin-coated pits at the cellular membranes [10]. MβCD disrupts cholesterol-rich microdomains and inhibits both caveola and lipid-raft-dependent endocytosis [11]. To determine the effects of the compounds on viral entry, HIV type-1 (HIV-1)-based pseudotype virus bearing VSV-G (VSV-G/HIVpv) was produced in 293T cells transfected with pCMV-VSV-G, pCAG-HIVgp and pCS-II-luc. Huh-7 cells were pretreated with various concentrations of compounds (PB1, chlorpromazine or MβCD) for 1 h at 37°C in a 48-well plate, inoculated with VSV-G/HIVpv at 5 ng/well of p24. After 4 h of inoculation, the cells were washed twice with phosphate-buffered saline (PBS) and treated with 0.25% trypsin-EDTA (Gibco BRL) at 37°C to degrade the unincorporated virus particles. Intracellular p24 of the HIV-1 gag protein was measured using a Retro-Tek HIV-1 p24 ELISA kit (ZeptoMetrix Copororation, Buffalo, NY, USA).

Time-of-addition assays

A time-of-addition experiment was carried out in Huh-7 cells. PB1 (100 μM) was added at 0, 1, 4, 8, 12 and 24 h after VSVpv or HCVpv infection in Huh-7 cells. The luciferase activity was measured after 48 h of infection as described previously [12,13].

Cytotoxicity assays

The cytotoxity of the compounds was examined using the Cell Counting Kit-8 (Dojindo Molecular Technologies, Inc., Kumamoto, Japan). Huh-7 cells were incubated with various concentrations of the compounds for 72 h to determine the cell viability. The 50% cytotoxicity concentration (CC_{50}) was defined as the concentration that reduced cell viability by 50%.

Flow cytometric analyses

Huh-7 cells were pretreated with or without PB1 (100 μM) at 37°C for 1 h. After washing with fluorescence-activated cell sorting (FACS) buffer (PBS with 2% fetal calf serum and 0.1% sodium azide), the cells were detached using 1 mM EDTA (Gibco BRL) for 30 min on ice. Cells were incubated with phycoerythrin (PE)-conjugated CD81 (Beckman Coulter, Fullerton, CA, USA) or CD71 (BD Pharmigen, San Diego, CA, USA) for 30 min at 4°C, subsequently washed and subjected to flow cytometry analysis (Cytomics FC500; Beckman Coulter). PE mouse immunoglobulin G2aκ monoclonal antibody (BD Pharmigen) was used as the isotype

Figure 1. Structures of PB1 and its components, and schematic diagrams of pseudotype viruses and the HCV replicon

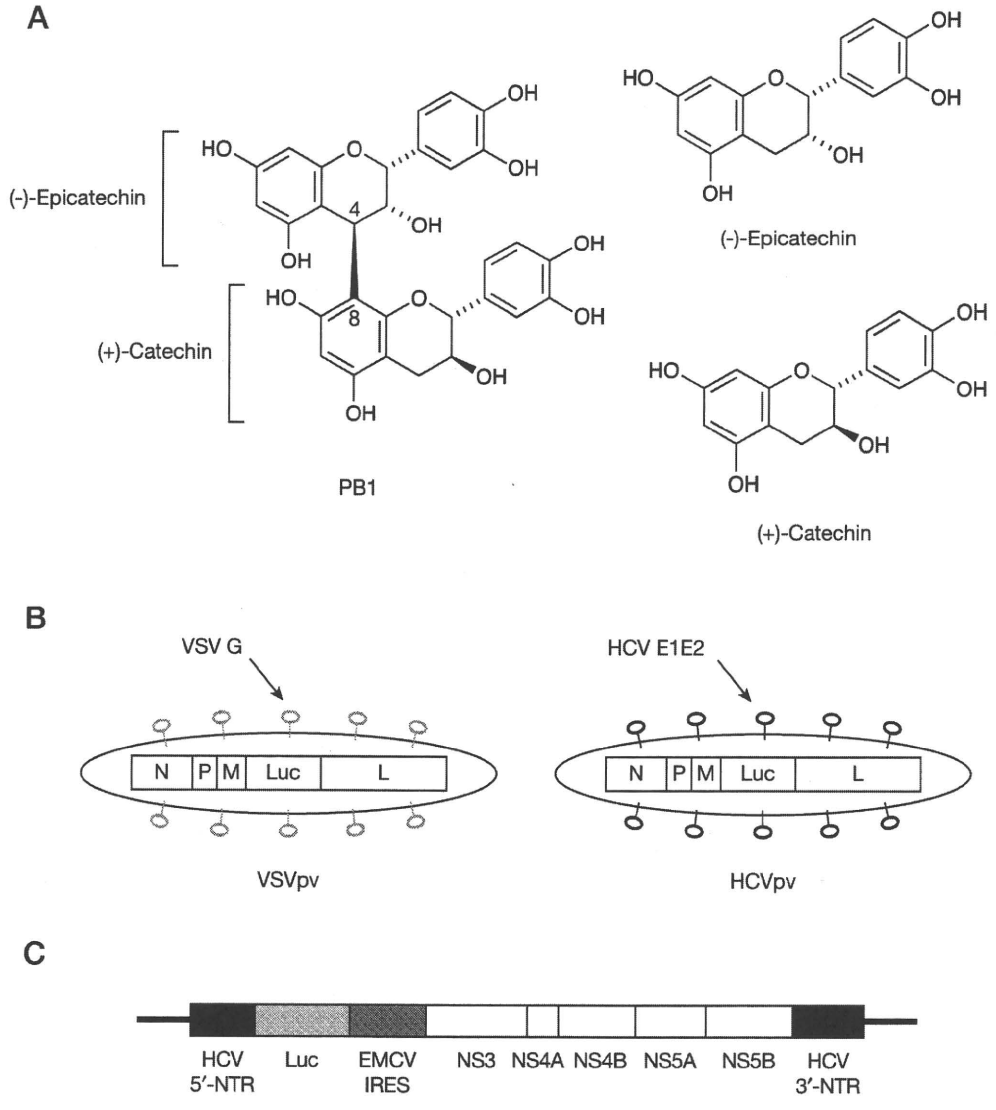

(A) Procyanidin B1 (PB1) are dimers composed of (-)-epicatechin and (+)-catechin by C4–C8 linkage. (B) Vesicular stomatitis virus (VSV) virus encodes five major proteins, which are nucleoprotein (N), phosphoprotein (P), matrix protein (M), glycoprotein (G) and large protein (L). Both VSV-based pseudotype viruses bearing hepatitis C virus (HCV) envelope proteins E1 and E2 (HCVpv) or VSV glycoprotein (VSVpv) contained the VSV genome, in which the G gene was replaced by the firefly luciferase reporter gene (Luc). (C) The HCV replicon contains the 5′-non-translated region (5′-NTR), the first 36 nucleotides of the core region fused directly with Luc, the internal ribosome entry site (IRES) element from encephalomyocarditis virus (ECMV) that directs translation of the HCV non-structural (NS) proteins from NS3 to NS5B and the 3′-NTR. 5′-NTR contains an IRES that is essential for cap-independent translation of HCV RNA. NS3 is a multifunctional protein with a serine protease and an RNA helixase/NTPase. The NS4A polypeptide functions as a cofactor for the NS3 serine protease. NS4B induces the formation of the membranous web. NS5A is a phosphoprotein that is important for HCV RNA replication. NS5B is RNA-dependent RNA polymerase.

control. 7-Amino-actinomycin (BD Pharmigen) was used as a viability probe for dead cell exclusion.

HCV replicon assays

The plasmid pLMH14 contains the 5′-non-translated region (5′-NTR), the first 36 nucleotides of the core region fused directly with the firefly luciferase reporter gene and the internal ribosome entry site (IRES) element from encephalomyocarditis virus (EMCV) that directs translation of the HCV non-structural (NS) proteins from NS3 to NS5B and the 3′-NTR as shown in Figure 1C. HCV replicon assays were performed as described previously [14]. Briefly, linearized pLMH14 at the restriction enzyme site *Xba*I was used for *in vitro* transcription of HCV replicon RNA using the SP6/T7 transcription kit (Roche, Mannheim, Germany).

Figure 2. Effects of PB1 on VSV-based pseudotype virus infection

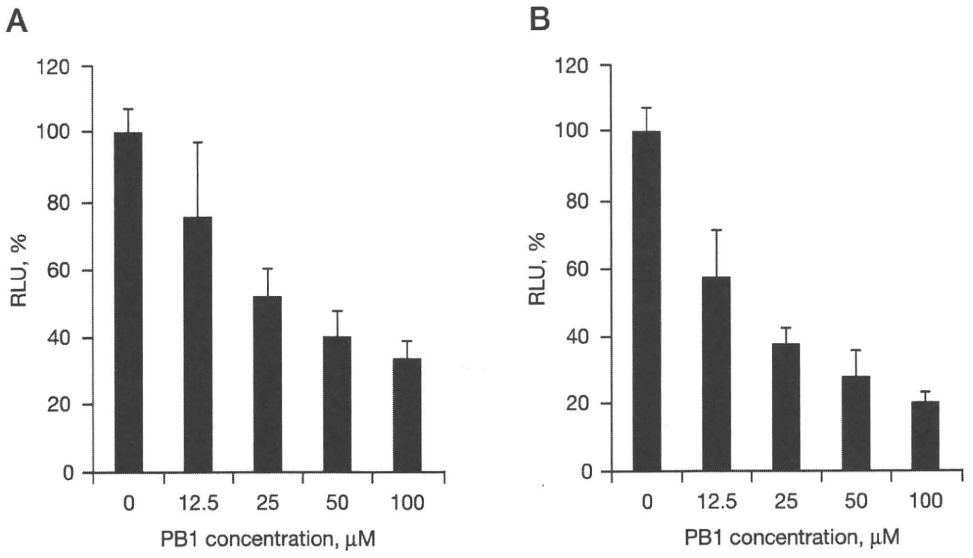

Huh-7 cells were pretreated with various concentrations of procyanidin B1 (PB1) for 1 h at 37°C. The cells were then infected by vesicular stomatitis virus (VSV)-based pseudotype viruses bearing **(A)** VSV glycoprotein or **(B)** hepatitis C virus envelope proteins E1 and E2 for 48 h. Experiments were performed in triplicate. The percentages of relative luciferase units (RLU; mean ±SD of three independent experiments) are shown.

Replicon RNA (0.5 μg) was transfected into Huh-7 cells in 24-well plates with lipofectamine 2000 (Invitrogen, Carlsbad, CA, USA). After 5 h, the medium was replaced and serially diluted PB1, ribavirin, (-)-epicatechin or (+)-catechin was added to Huh-7 cells. The luciferase activity was determined at 3 h and 72 h post-transfection. The luciferase activities at 3 h were used for normalization of the transfection efficiency.

Semi-quantitative RT-PCR

At 24 h prior to transfection of HCV replicon RNA (0.5 μg), Huh-7 cells were seeded at a density of 2×10^5 cells/well in 12-well plates. After 72 h of PB1 treatment, total cellular RNA was extracted using TRIzol reagent (Invitrogen) and subjected to reverse transcription coupled PCR (RT-PCR) with a One Step RNA PCR kit (TaKaRa Bio, Inc., Shiga, Japan). Reactions were incubated at 50°C for 30 min for reverse transcription, for 2 min at 94°C to inactivate the avian myeloblastosis virus reverse transcriptase and subsequent PCR amplification of 30 cycles of denaturation at 94°C for 30 s, annealing at 55°C for 15–45 s and extension at 72°C for 1 min.

5′-NTR and firefly luciferase genes in the HCV replicon RNA (Figure 1C) and cellular β-actin were amplified with the following primers: 5′-NTR (forward 5'-ACACTCCACCATAGATCACTCCCCT-3' and reverse 5'-CGGGGCACTCGCAAGCACCCTATCA-3'), firefly luciferase (forward 5'-CACATCTCATCTACCTCCCG-3' and reverse 5'-TCCACAACCTTCGCTTCA-3') and β-actin (forward 5'-ATCTGGCACCACACCTTCTACAATGAGCTGCG-3' and reverse 5'-CGTCATACTCCTGCTTGCTGATCCACATCTGC-3').

Results

PB1 suppressed VSVpv and HCVpv infection

A pseudotype virus can make only a single round of infection without producing infectious progeny virus in infected cells, making it an excellent system for studying the viral replication steps between entry and RNA genome synthesis. Two pseudotype viruses were used: VSVpv comprising VSV envelope protein G and *env*-deleted VSV genome (ΔG-VSV), and HCVpv comprising HCV E1E2 and ΔG-VSV. The only difference between VSVpv and HCVpv is the envelope (Figure 1B). In this assay, PB1 inhibited both VSVpv and HCVpv infection in a dose-dependent manner (Figure 2). The mean ±SD EC_{50} for VSVpv and HCVpv was 29 ±7.3 μM and 15 ±3.9 μM, respectively. These results indicate that PB1 blocks VSV and HCV pseudotype virus infection by interference with the viral entry step through HCV or VSV envelope proteins and/or intracellular VSV genome replication process.

PB1 inhibited viral replication at post-entry step(s)

To determine the mechanism of action of PB1 on HCV replication, a time of addition experiment was performed.

Figure 3. Time of addition analysis of PB1 in Huh-7 cells

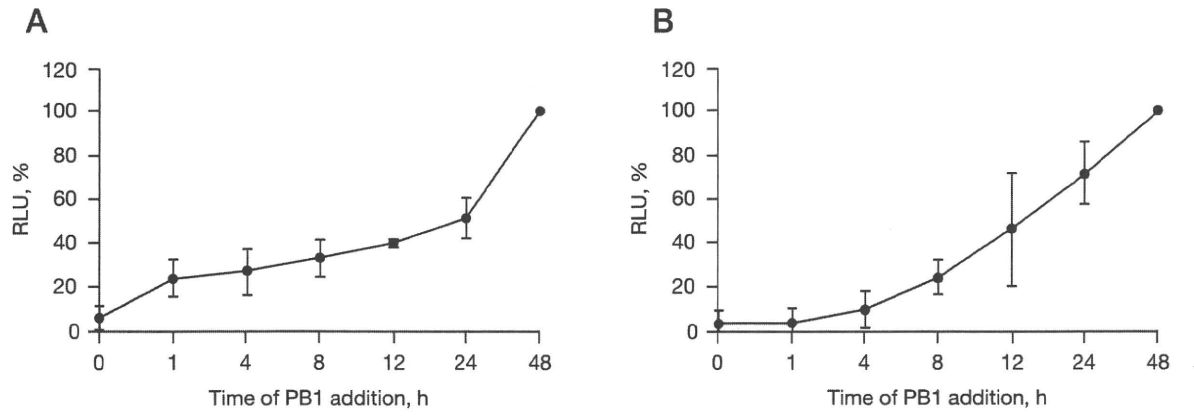

Procyanidin B1 (PB1; 100 μM) was added at the indicated time points (0, 1, 4, 8, 12 and 24 h) after infection with **(A)** vesicular stomatitis virus glycoprotein or **(B)** hepatitis C virus envelope proteins E1 and E2 in Huh-7 cells. The luciferase activity in the cells was measured up to 48 h infection. Relative luciferase units (RLUs) at 48 h was defined as 100%. Experiments were performed in triplicate. Results represent the mean ±SD of three independent experiments.

Table 1. Flow cytometric analysis of CD81 expression

PB1	CD81-positive staining cells, %	MFI	CD71-positive staining cells, %	MFI
Negative	96.5	9.53	98.1	11.8
Positive	95.2	9.50	96.5	11.6

Huh-7 cells were pretreated with or without procyanidin B1 (PB1; 100 μM) at 37°C for 1 h. Cells were washed, detached, incubated with phycoerythrin-conjugated CD81 or CD71 (transferrin receptor) for 30 min at 4°C and then subjected to flow cytometric analysis. Positive-staining cells and mean fluorescence intensity (MFI) are shown.

The assay provided time-dependent activity that enabled estimation of the inhibitory step(s) of compounds. As shown in Figure 3, the luciferase activity was suppressed to <50% even when PB1 was added after 12 h of VSVpv or HCVpv pseudotype virus infection. A previous study showed that nearly 90% of VSV and HCV was internalized into Huh-7 cells within 1.5 and 3 h, respectively [15]. These results suggest that PB1 blocks viral replication after the internalization.

PB1 had no inhibitory effects on viral entry

To further determine whether PB1 affects the expression of CD81, one of the main receptors of HCV [16], flow cytometric assays were performed. CD71 (transferrin receptor) was used as a negative control as PB1 does not affect CD71 expression [7]. The proportion of positive-staining cells and mean fluorescence intensity (MFI) were little changed by PB1 treatment (Table 1).

Entry of both VSV and HCV depends on clathrin-dependent endocytosis [10,17]. To examine the effects on viral entry, we therefore used VSV-G/HIVpv. After 4 h of infection during the reverse transcription step of the HIV-1 genome, we determined the amount of intracellular HIV-1 gag protein p24, which is highly correlated with that of entered virus particles [18]. Consistent with previous reports [11], chlorpromazine decreased the intracellular p24 level in a dose-dependent manner (Figure 4A), whereas MβCD did not (Figure 4B). PB1 had little effect on the intracellular p24 levels (Figure 4C). Moreover, the binding of VSV-G/HIVpv at 4°C was maintained even in the presence of PB1 (Figure 4D). These results indicate that PB1 inhibits the virus infection rather than the entry; thus, at least for HCV and VSV infection, it is unlikely that PB1 blocks viral replication through inhibition of clathrin-dependent endocytosis.

PB1 inhibited HCV RNA synthesis

We next examined the effects of PB1 on HCV RNA replication. Although ribavirin has been shown to inhibit RNA synthesis *in vivo*, it has little effect on HCV RNA replication in the replicon system *in vitro* [19]. Consistent with the previous report, the inhibitory effect of ribavirin seems to be induced by its cytotoxity (Figure 5A); however, PB1 suppressed the replication of HCV replicon in a dose-dependent manner (Figure 5B). The mean ±SD EC_{50} and CC_{50} values were 72 ±7.4 μM and 465 ±79 μM,

respectively, with the result that the selective index (CC_{50}/EC_{50}) was calculated to be 6.5. Because PB1 is composed of (-)-epicatechin and (+)-catechin by C4–C8 linkage (Figure 1A), we next examined both components solely for anti-HCV activity. The single components, (-)-epicatechin or (+)-catechin, had little inhibitory effects on HCV replicon (Figure 5C and 5D) indicating that the dimer structure of PB1 is required for inhibitory activity.

The effects of PB1 on the synthesis of HCV RNA in the cells were examined by semi-quantitative RT-PCR. As shown in Figure 6, the signal intensity for 5′-NTR and luciferase correlated with the amount of intracellular HCV RNA copies; the signal intensity was weak at higher concentrations (100 μM and 50 μM of PB1) compared with the signal intensity at lower concentrations. In parallel experiments, the signal intensity for β-actin was little changed up to 100 μM PB1 indicating that PB1 directly inhibited the intracellular HCV RNA replication without affecting cellular messenger RNA synthesis. These results demonstrated that PB1 blocks HCV replication through the inhibition of RNA synthesis.

Discussion

Procyanidins, which are oligomers and/or polymers of monomeric flavonoids, exert strong antioxidant and

Figure 4. PB1 inhibits VSV-G/HIVpv binding and endocytosis in Huh-7 cells

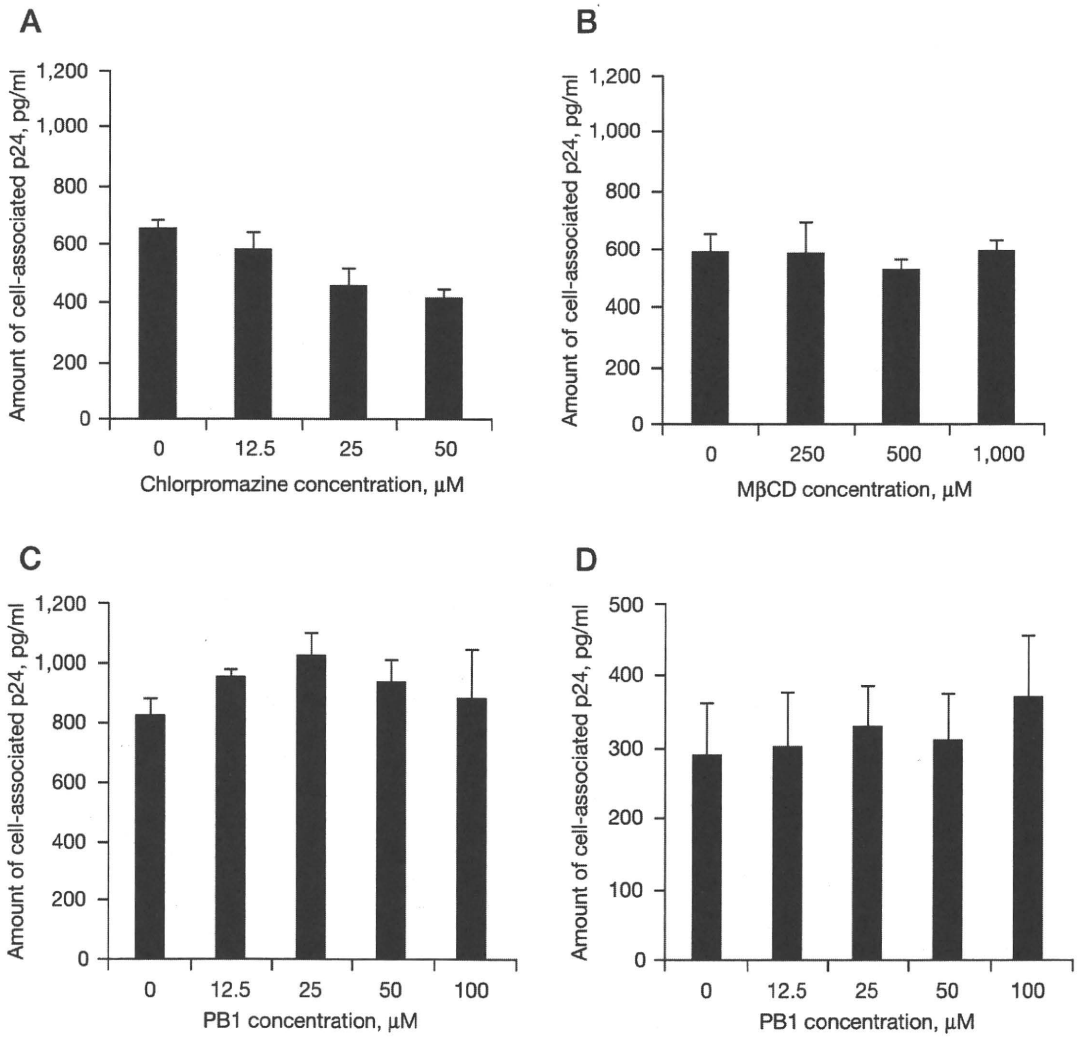

Huh-7 cells were pretreated with various concentrations of (A) chlorpromazine, (B) methyl-β-cyclodextrin (MβCD) or (C) procyanidin B1 (PB1) for 1 h at 37°C. The cells were then infected with HIV type-1-based pseudotype virus bearing the vesicular stomatitis virus envelope protein G (VSV-G/HIVpv; 5 ng of p24) at 37°C for 4 h. To determine the effects on viral binding, Huh-7 cells were incubated with (D) PB1 and VSV-G/HIVpv (5 ng of p24) on ice for 4 h. Results represent the mean ±SD of three independent assays.

radical scavenging activity compared with vitamins C and E [20]. A procyanidin derivative, PB1, purified from *Cinnamomi cortex* has inhibitory effects on the replication of herpes simplex virus [21], HIV-1 [22] and SARS-CoV [7]. However, to date, the anti-HCV activity of PB1 has not been documented; therefore, in this study, we examined the effects of PB1 on HCV replication and revealed that PB1 inhibited HCV replication. Procyanidins have many isomeric forms depending on the extent of polymerization (dimers to pentadecamers) and the nature of their constituent units [23]. Some biological activities are related to the degree of polymerization. In our study, (-)-epicatechin and (+)-catechin, which are components of PB1, alone showed little anti-HCV activity indicating that the polymerization of catechins plays an important role in antiviral activity.

The currently recommended therapy for chronic hepatitis C is a combination of PEG-IFN and ribavirin for 24 or 48 weeks. IFN has potent antiviral activity but indirectly inhibits viral replication. Rather, it induces IFN-stimulated genes, which establish a non-virus-specific antiviral state in the cell [19]. Several possible mechanisms of action of ribavirin in HCV have been proposed including: inhibition of inosine monophosphate dehydrogenase, leading to depletion of guanosine triphosphate (GTP) necessary for viral

Figure 5. PB1 inhibits HCV replication

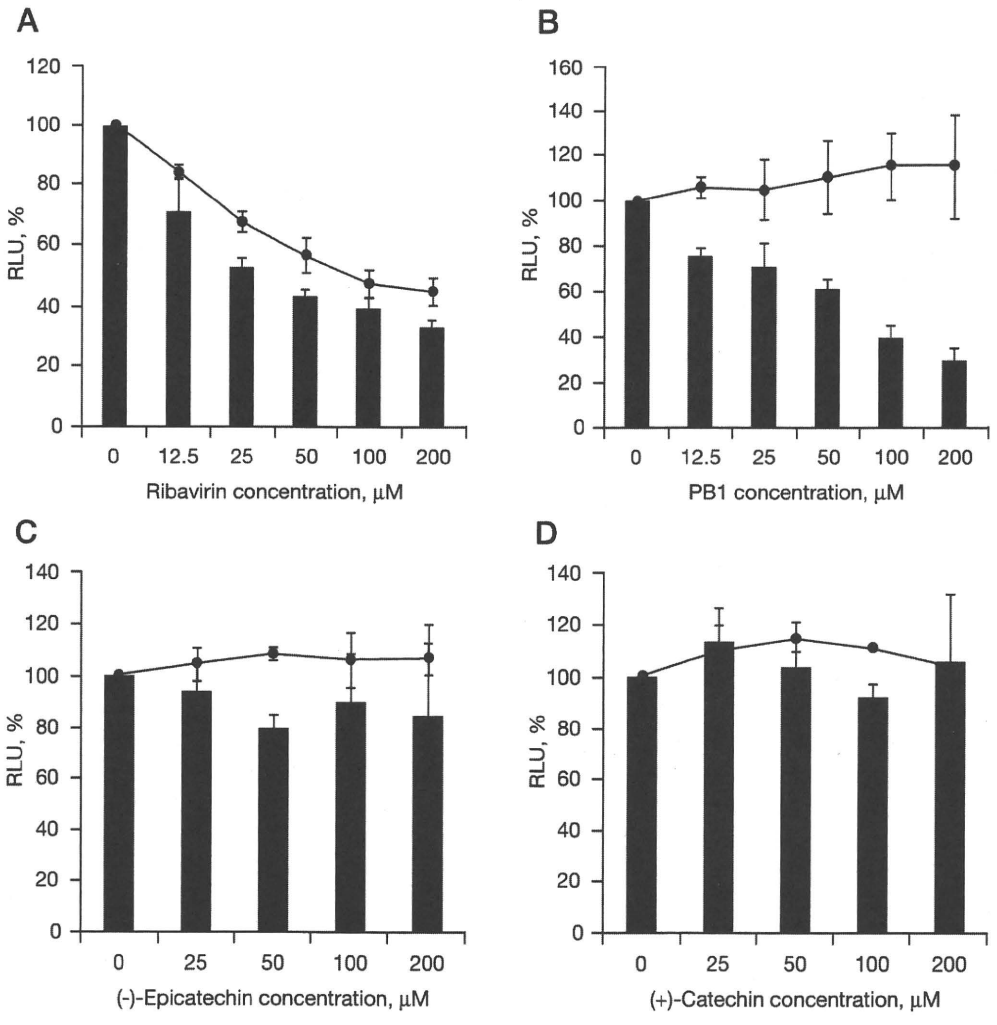

In vitro transcribed hepatitis C virus (HCV) replicon RNAs were transfected into Huh-7 cells. After 5 h, various concentrations of **(A)** ribavirin, **(B)** procyanidin B1 (PB1), **(C)** (-)-epicatechin and **(D)** (+)-catechin were added to the transfected cells. Luciferase activities were measured at 72 h post-transfection. Relative luciferase units (RLUs) at 72 h in the cells without compounds were defined as 100%. Experiments were performed in triplicate. Results represent the mean ±SD from at least three independent experiments. The black bars represent the inhibition of HCV replication and the lines represent the cytotoxicity of each compound.

RNA synthesis [24,25]; induction of lethal mutagenesis in the viral RNA genome [26,27]; and alteration of the T_H1/ T_H2 balance favouring a T_H1 $CD4^+$ T-cell response and thus leading to viral clearance [19,28]. Some studies also demonstrated that ribavirin directly inhibits HCV RNA polymerase *in vitro* [19,25,29]. The guanosine analogue, ribavirin, is intracellularly phosphorylated into triphosphate forms that act as a chain terminator through misincorporation of ribavirin triphosphate by HCV RNA polymerase, resulting in the inhibition of HCV replication. However, it is unlikely to be its major mechanism of action against HCV *in vivo*. By contrast, the mechanism of action of PB1 appears to be distinct from those of IFN and ribavirin. In our study, PB1 inhibited both VSV and HCV pseudotype virus infection in Huh-7 cells. PB1 interfered little with viral entry but inhibited HCV RNA synthesis in a dose-dependent manner. It is possible that PB1 inhibits other targets including cellular factors required for RNA synthesis. However, PB1 can selectively block HCV RNA synthesis without influence on cellular RNA (β-actin) synthesis; therefore, it is likely that PB1 suppresses HCV RNA synthesis as a HCV RNA polymerase inhibitor. Unfortunately, HCV RNA dependent RNA polymerase is not commercially available at present. To strengthen our hypothesis, we examined whether PB1 inhibits the polymerase activity of the T7 RNA polymerase in an enzymetic assay and demonstrated that PB1 directly inhibits T7 RNA polymerase activity (SL *et al.*, data not shown). The effects of PB1 on NS3 helicase or NS3/4A serine protease will also need to be determined because the inhibition of helicase or protease can lead to the suppression of HCV RNA synthesis. Further experiments are needed to reveal the detailed mechanisms of HCV inhibition in future; however, at present, HCV enzymes mentioned above are not commercially available.

In contrast to tumour viruses that cause tumourigenesis, such as human T-cell lymphotropic virus type-1 and hepatitis B virus (HBV), the HCV genome is not integrated into its host genome and has a predominantly cytoplasmic life cycle [30]. Although the mechanisms of tumourigenesis still remain unclear, chronic immune-mediated inflammation and associated oxidative chromosomal DNA damage probably play an important role in HCV-induced hepatocellular carcinoma [31,32]. Procyanidins inhibit tumour growth and induce apoptosis in various tumour cells [23,33,34]. One of the possible mechanisms of the suppressive effects on carcinogenesis appears to be antioxidant and anti-inflammatory activities suggesting that procyanidins might prevent the development of HCV-related hepatocellular carcinoma. Procyanidins, abundant in natural plant products including berries, grapes, cinnamon and pycnogenol, have few adverse effects on normal cells compared with current therapeutic agents [35] suggesting that they could be good candidates as additional or supportive anti-HCV agents used in prolonged therapy.

Figure 6. Expression of messenger RNA by RT-PCR

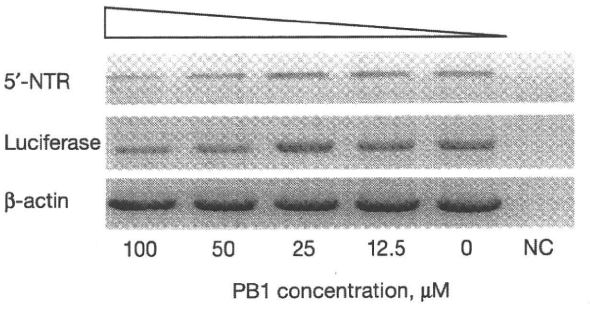

Hepatitis C virus (HCV) replicon transfected Huh-7 cells were incubated in the absence or presence of various concentrations of procyanidin B1 (PB1). After 72 h, total RNA was extracted from the cells and subjected to reverse transcription (RT)-PCR amplification of the 5′-non-translated region (5′-NTR), luciferase gene and β-actin. The amplified products were visualized by ethidium bromide straining. NC, negative control.

Several studies showed that procyanidins can be absorbed in rats and humans [36–39]. Procyanidins were detected in the human plasma as early as 30 min and reached the maximal concentrations by 2 h after oral administration [38]. Holt *et al.* [38] reported that 2 h after the ingestion of a procyanidin-rich cocoa (0.375 g/kg) containing 256 mg procyanidin, the concentration of procyanidin B2 in human plasma reached 41 nM on average, indicating that oral administration of 62 g of cocoa procyanidins is needed to reach a plasma concentration of 10 μM. In another study, the concentrations of procyanidin B2 in human plasma reached 100 nM after the consumption of cocoa (0.5 g/kg), of which 9.7 mg/g was procyanidins [39], indicating that 38 g of cocoa procyanidins is required to reach a plasma concentration of 10 μM at 2 h after oral administration. PB1 showed moderate antiviral activity not only in our study but also in other studies [7,21,22], which reported antiviral activity at concentrations (1–100 μM). To improve the physiological concentration, certain chemical modifications that enhance antiviral activity, plasma stability and/or absorption of PB1 are required. The development of drug delivery systems might also enable to improve bioavailability and antiviral efficiency.

In this study, we demonstrated that a catechin dimer from natural plants, PB1, suppresses HCV RNA synthesis possibly as a HCV RNA polymerase inhibitor. Our study could contribute to the development of novel therapeutic strategies for the prevention and treatment of HCV as well as other viral infections.

Acknowledgements

This work was supported, in part, by Grants-in-Aid for Special Educational Grant from the Ministry of Education, Culture, Sports, Science, and Technology, and for the Scientific Research Expenses from the Ministry of Health, and Welfare (Japan). LS has been supported by the Japanese AIDS Foundation (Tokyo, Japan).

Disclosure statement

The authors declare no competing interests.

References

1. Lauer GM, Walker BD. Hepatitis C virus infection. *N Engl J Med* 2001; **345**:41–52.
2. NIH Consensus statement on management of hepatitis C: 2002. *NIH Consens State Sci Statements* 2002; **19**:1–46.
3. Fried MW, Shiffman ML, Reddy KR, *et al.* Peginterferon alfa-2a plus ribavirin for chronic hepatitis C virus infection. *N Engl J Med* 2002; **347**:975–982.
4. Manns MP, McHutchison JG, Gordon SC, *et al.* Peginterferon alfa-2b plus ribavirin compared with interferon alfa-2b plus ribavirin for initial treatment of chronic hepatitis C: a randomised trial. *Lancet* 2001; **358**:958–965.
5. Reesink HW, Zeuzem S, Weegink CJ, *et al.* Rapid decline of viral RNA in hepatitis C patients treated with VX-950: a Phase Ib, placebo-controlled, randomized study. *Gastroenterology* 2006; **131**:997–1002.
6. Li H, Tatlock J, Linton A, *et al.* Discovery of (R)-6-cyclopentyl-6-(2-(2,6-diethylpyridin-4-yl)ethyl)-3-((5,7-dimethyl- [1,2,4]triazolo[1,5-a]pyrimidin-2-yl)methyl)-4-hydroxy-5,6-dihydropyran-2-one (PF-00868554) as a potent and orally available hepatitis C virus polymerase inhibitor. *J Med Chem* 2009; **52**:1255–1258.
7. Zhuang M, Jiang H, Suzuki Y, *et al.* Procyanidins and butanol extract of Cinnamomi cortex inhibit SARS-CoV infection. *Antiviral Res* 2009; **82**:73–81.
8. Tanaka T, Matsuo Y, Yamada Y, Kouno I. Structure of polymeric polyphenols of cinnamon bark deduced from condensation products of cinnamaldehyde with catechin and procyanidins. *J Agric Food Chem* 2008; **56**:5864–5870.
9. Tani H, Komoda Y, Matsuo E, *et al.* Replication-competent recombinant vesicular stomatitis virus encoding hepatitis C virus envelope proteins. *J Virol* 2007; **81**:8601–8612.
10. Blanchard E, Belouzard S, Goueslain L, *et al.* Hepatitis C virus entry depends on clathrin-mediated endocytosis. *J Virol* 2006; **80**:6964–6972.
11. Inoue Y, Tanaka N, Tanaka Y, *et al.* Clathrin-dependent entry of severe acute respiratory syndrome coronavirus into target cells expressing ACE2 with the cytoplasmic tail deleted. *J Virol* 2007; **81**:8722–8729.
12. Kodama EI, Kohgo S, Kitano K, *et al.* 4′-Ethynyl nucleoside analogs: potent inhibitors of multidrug-resistant human immunodeficiency virus variants in vitro. *Antimicrob Agents Chemother* 2001; **45**:1539–1546.
13. Okamoto M, Fujiwara M, Kodama E, *et al.* Inhibition of human immunodeficiency virus replication by RD6-Y664, a novel benzylhydroxylamine derivative. *Antivir Chem Chemother* 1999; **10**:71–77.
14. Zhang J, Yamada O, Kawagishi K, *et al.* Up-regulation of hepatitis C virus replication by human T cell leukemia virus type I-encoded Tax protein. *Virology* 2007; **369**:198–205.
15. McHutchison JG, Everson GT, Gordon SC, *et al.* Telaprevir with peginterferon and ribavirin for chronic HCV genotype 1 infection. *N Engl J Med* 2009; **360**:1827–1838.
16. Cormier EG, Tsamis F, Kajumo F, Durso RJ, Gardner JP, Dragic T. CD81 is an entry coreceptor for hepatitis C virus. *Proc Natl Acad Sci U S A* 2004; **101**:7270–7274.
17. Sun X, Yau VK, Briggs BJ, Whittaker GR. Role of clathrin-mediated endocytosis during vesicular stomatitis virus entry into host cells. *Virology* 2005; **338**:53–60.
18. Haga S, Yamamoto N, Nakai-Murakami C, *et al.* Modulation of TNF-alpha-converting enzyme by the spike protein of SARS-CoV and ACE2 induces TNF-alpha production and facilitates viral entry. *Proc Natl Acad Sci U S A* 2008; **105**:7809–7814.
19. Feld JJ, Hoofnagle JH. Mechanism of action of interferon and ribavirin in treatment of hepatitis C. *Nature* 2005; **436**:967–972.
20. Shi J, Yu J, Pohorly JE, Kakuda Y. Polyphenolics in grape seeds – biochemistry and functionality. *J Med Food* 2003; **6**:291–299.
21. Feng WY, Tanaka R, Inagaki Y, *et al.* Pycnogenol, a procyanidin-rich extract from French maritime pine, inhibits intracellular replication of HIV-1 as well as its binding to host cells. *Jpn J Infect Dis* 2008; **61**:279–285.
22. De Bruyne T, Pieters L, Witvrouw M, De Clercq E, Vanden Berghe D, Vlietinck AJ. Biological evaluation of proanthocyanidin dimers and related polyphenols. *J Nat Prod* 1999; **62**:954–958.
23. Miura T, Chiba M, Kasai K, *et al.* Apple procyanidins induce tumor cell apoptosis through mitochondrial pathway activation of caspase-3. *Carcinogenesis* 2008; **29**:585–593.
24. Dixit NM, Perelson AS. The metabolism, pharmacokinetics and mechanisms of antiviral activity of ribavirin against hepatitis C virus. *Cell Mol Life Sci* 2006; **63**:832–842.
25. Lau JY, Tam RC, Liang TJ, Hong Z. Mechanism of action of ribavirin in the combination treatment of chronic HCV infection. *Hepatology* 2002; **35**:1002–1009.
26. Crotty S, Cameron CE, Andino R. RNA virus error catastrophe: direct molecular test by using ribavirin. *Proc Natl Acad Sci U S A* 2001; **98**:6895–6900.
27. Vignuzzi M, Stone JK, Andino R. Ribavirin and lethal mutagenesis of poliovirus: molecular mechanisms, resistance and biological implications. *Virus Res* 2005; **107**:173–181.
28. Tam RC, Pai B, Bard J, *et al.* Ribavirin polarizes human T cell responses towards a Type 1 cytokine profile. *J Hepatol* 1999; **30**:376–382.
29. Bougie I, Bisaillon M. Initial binding of the broad spectrum antiviral nucleoside ribavirin to the hepatitis C virus RNA polymerase. *J Biol Chem* 2003; **278**:52471–52478.
30. Suzuki T, Ishii K, Aizaki H, Wakita T. Hepatitis C viral life cycle. *Adv Drug Deliv Rev* 2007; **59**:1200–1212.
31. Bartosch B, Thimme R, Blum HE, Zoulim F. Hepatitis C virus-induced hepatocarcinogenesis. *J Hepatol* 2009; **51**:810–820.
32. McGivern DR, Lemon SM. Tumor suppressors, chromosomal instability, and hepatitis C virus-associated liver cancer. *Annu Rev Pathol* 2009; **4**:399–415.
33. Hsu CP, Lin YH, Chou CC, *et al.* Mechanisms of grape seed procyanidin-induced apoptosis in colorectal carcinoma cells. *Anticancer Res* 2009; **29**:283–289.
34. Mantena SK, Baliga MS, Katiyar SK. Grape seed proanthocyanidins induce apoptosis and inhibit metastasis of highly metastatic breast carcinoma cells. *Carcinogenesis* 2006; **27**:1682–1691.
35. Ye X, Krohn RL, Liu W, *et al.* The cytotoxic effects of a novel IH636 grape seed proanthocyanidin extract on cultured human cancer cells. *Mol Cell Biochem* 1999; **196**:99–108.
36. Appeldoorn MM, Vincken JP, Gruppen H, Hollman PC. Procyanidin dimers A1, A2, and B2 are absorbed without conjugation or methylation from the small intestine of rats. *J Nutr* 2009; **139**:1469–1473.
37. Baba S, Osakabe N, Natsume M, Terao J. Absorption and urinary excretion of procyanidin B2 [epicatechin-(4β-8)-epicatechin] in rats. *Free Radic Biol Med* 2002; **33**:142–148.